Dominance reversal maintains large-effect resistance polymorphism in temporally varying environments

Marianthi Karageorgi[1,7], Anastasia S. Lyulina[1,2], Mark C. Bitter[1], Egor Lappo[1], Sharon I. Greenblum[3], Zach K. Mouza[1], Caitlynn T. Tran[1], Andy V. Huynh[1], Hayes Oken[4], Paul Schmidt[4,6,7], and Dmitri A. Petrov[1,5,6,7]

1. Department of Biology, Stanford University, Stanford, CA 94305, USA
2. Department of Applied Physics, Stanford University, Stanford, CA 94305, USA
3. Department of Energy Joint Genome Institute, Lawrence Berkeley National Laboratory, Berkeley, CA 94720, USA
4. Department of Biology, University of Pennsylvania, Philadelphia, PA 19104, USA
5. CZ Biohub, San Francisco, CA 94158
6. These authors contributed equally
7. Corresponding authors: M.K. (mkarag@stanford.edu), P.S. (schmidtp@upenn.edu), and D.A.P (dpetrov@stanford.edu)

Abstract

A central challenge in evolutionary biology is to uncover mechanisms maintaining functional genetic variation[1]. Theory suggests that dominance reversal, whereby alleles subject to fluctuating selection are dominant when beneficial and recessive when deleterious, can help stabilize large-effect functional variation in temporally varying environments[2,3]. However, empirical evidence for dominance reversal is scarce because testing requires both knowing the genetic architecture of relevant traits and measuring the dominance effects on fitness in natural conditions[4]. Here, we show that large-effect, insecticide-resistance alleles at the *Ace* locus in *Drosophila melanogaster*[5,6] persist worldwide at intermediate frequencies and exhibit dominance reversal in fitness as a function of the presence of an organophosphate insecticide. Specifically, we use laboratory assays to show that the resistance benefits driven by these alleles are dominant, while the associated costs are recessive (or codominant). Further, by tracking insecticide resistance and genome-wide allele frequencies in field mesocosms, we find that resistance and resistant alleles increase and then decrease rapidly in response to an insecticide pulse but are maintained at low frequencies in the absence of pesticides. We argue that this pattern is only consistent with beneficial reversal of dominance. We use Wright's theory of dominance[7] to hypothesize that dominance reversal should be common in general if the environmental shifts that make alleles deleterious also make them behave effectively as loss-of-function and thus recessive alleles . We also use the known haplotype structure of mesocosm populations to establish that the insecticide pulse generates chromosome-scale genomic perturbations of allele frequencies at linked sites. Overall, our results provide compelling evidence that this mechanism can maintain functional genetic variation and

42 **enable rapid adaptation to environmental shifts that can impact patterns of genomic**

43 **variation at genome-wide scales via linked fluctuating selection.**

Main text

The maintenance of functional genetic variation at large-effect loci for fitness-related traits in natural populations is a fundamental paradox[8,9]. Directional selection should in principle rapidly erode such variation. Yet many systems show persistence of such large effect loci at intermediate frequencies suggesting the action of some form of balancing selection[10,11]. A particularly striking example comes from studies of seasonal dynamics in *Drosophila*, which revealed the presence of large-effect seasonal polymorphisms[12,13] that rapidly respond to environmental fluctuations shifting between advantageous to deleterious multiple times during a single seasonal cycle[14,15]. Some of these seasonal alleles have strong enough selective effects that they can change frequencies by tens of percent per season, yet still remain polymorphic over hundreds of thousands or even millions of generations[12]. Polymorphisms of large effect responding to fluctuating selection have been observed in a wide range of other systems including other insects[16–19], fish[20,21], mammals[22,23], and plants[24]. In all these examples the alternative alleles are subject to strong antagonistic and fluctuating selection that could help maintain large-effect polymorphisms in the overall population by generating effective overdominance. Theoretical models suggest that fluctuating selection can indeed stabilize genetic variation in the face of temporally varying selection especially if combined with beneficial dominance reversal[2,3,25].

Under beneficial dominance reversal, alleles are partially or completely dominant when beneficial, but then become partially or completely recessive when deleterious[26,27]. This mechanism acts as a stabilizing force because it protects recessive deleterious alleles from selection and slows down their loss. At the same time, it allows a rapid response to selection

66 shifts, as adaptive alleles are always dominant and thus quickly respond to selection even when
67 rare. Even modest dominance reversals have been shown to protect variation under fluctuating
68 selection in single- or multiple-locus models[3]. However, it remains unknown how often the
69 beneficial dominance reversal occurs in nature for functional polymorphic large-effect loci and
70 whether it arises naturally within genetic systems. The scarcity of relevant adaptive traits with a
71 known genetic architecture, and the challenges of measuring fitness and dominance effects in
72 natural environments, make these questions difficult to address.

73 Importantly, models of fluctuating selection that incorporate beneficial dominance
74 reversal of large-effect alleles predict stable, large-amplitude fluctuations at the adaptive locus
75 and thus could drive significant effects on linked genomic variation[28,29]. These effects on linked
76 sites can extend across large genomic distances, with their magnitude directly proportional to
77 how rapidly the adaptive allele frequencies shift[30]. These long-range effects of strong fluctuating
78 selection have rarely been quantified, as the haplotype structure of adaptive alleles at a selected
79 locus is typically not known and the linked selection becomes virtually undetectable in standing
80 genetic data for old and common alleles present on multiple haplotypes.

81 Here we investigate the dominance of large-effect alleles conferring resistance to
82 organophosphate insecticides at the *Ace* locus in natural populations of *Drosophila melanogaster*
83 both in organophosphate-rich and -free environments. *Ace* encodes acetylcholinesterase (AChE),
84 a key enzyme in the insect nervous system responsible for breaking down acetylcholine[31].
85 Organophosphate insecticides, introduced in the 1950s and 1960s, act as irreversible inhibitors of
86 AChE, causing insect death by binding to its active site and preventing removal of acetylcholine
87 from the synapses upon firing[32]. These insecticides have imposed seasonally fluctuating selection
88 pressures on *D. melanogaster* populations, as seen in seasonal resistance fluctuations in field

89 studies[33,34]. Therefore, this case provides a compelling example of a large-effect polymorphism
90 subject to fluctuating selection, in which the causal locus, the mechanistic basis of selection, and
91 the conditions that favor alternative alleles are well understood.

92 To understand how selection maintains resistant *Ace* alleles in nature, we first analyzed
93 genomic data from worldwide *D. melanogaster* populations from the Drosophila Evolution Over
94 Space and Time (DEST) database[35] and country-level pesticide use data from the Food and
95 Agricultural Organization of the United Nations (FAO)[36] for the period of 2000-2022. Previous
96 studies identified resistant *Ace* alleles in *D. melanogaster* with mutations at four conserved sites
97 near the AChE active site (I161V, G265A, F330Y, G368A), with VGFG and VAYG being the
98 most common resistance haplotypes[5,6] (inset, **Fig. 1a**). Our analysis of two panels of inbred lines
99 collected in an orchard in Pennsylvania (LNPA[14]) and a farmer's market in North Carolina
100 (DGRP[37]) confirmed these as the most common resistant haplotypes in resistant *Ace* alleles
101 (**Extended Data Fig. 1a, b**). The LNPA population also carries the VGFA haplotype at ~13%
102 frequency. For our analysis, we used the shared I161V resistance polymorphism as a marker for
103 all three resistant *Ace* alleles.

104 We found evidence for spatially and temporally varying selection on the I161V
105 polymorphism. Spatially, its frequency increases with pesticide use intensity across countries
106 (linear mixed-effect model, $p = 0.006$) (**Fig. 1a, b**) and shows stronger spatial variation
107 compared to control SNPs matched for recombination and average frequency ($p = 0.005$) (**Fig.**
108 **1c**). Temporally, analyzing seasonal frequency patterns at Linvilla Orchards, a non-organic farm
109 where samples were collected in spring and fall between 2009 and 2015, we found a consistent
110 decline in I161V frequency when comparing available fall samples paired to the following spring
111 (generalized linear model, $p = 0.005$), suggesting either fitness costs in the absence of

insecticides during winter or seasonal migration (**Fig. 1d**). In addition, we found that the I161V polymorphism shows stronger temporal fluctuations than control SNPs (p = 0.053) (**Fig. 1e).**

Figure 1

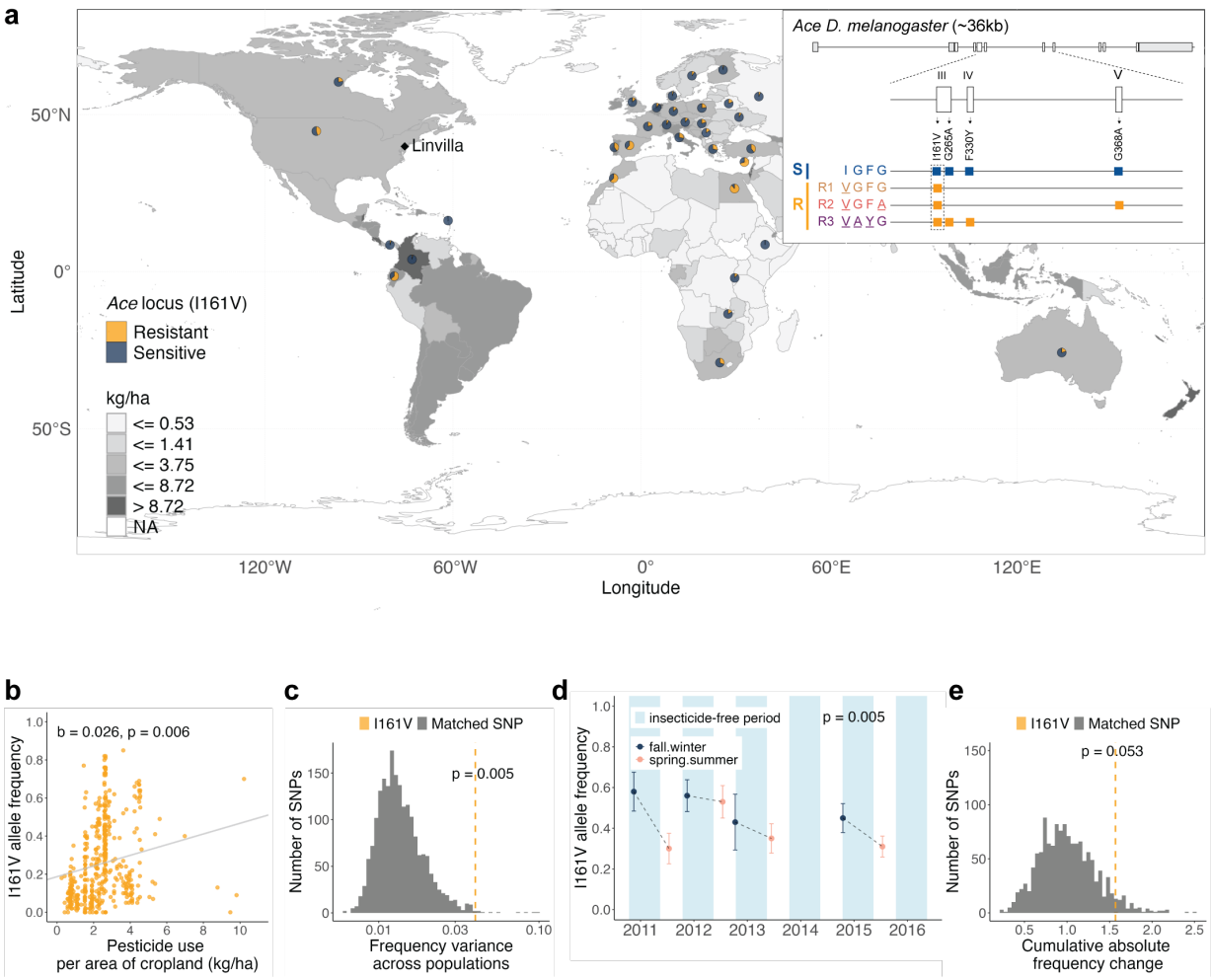

Figure 1. Organophosphate-resistant *Ace* alleles persist at intermediate frequencies in natural *Drosophila melanogaster* populations and respond to spatial and seasonal insecticide selection. a, Allele frequency map of I161V (pie charts), a marker of organophosphate-resistant *Ace* alleles, overlaid on insecticide use intensity (shading). Inset shows common resistant *Ace* alleles with three different resistance haplotypes (R1: VGFG, R2: VGFA, R3: VAYG) in *D. melanogaster* (See also **Extended Data Fig. 1** for frequencies of resistant haplotypes in DGRP and LNPA panels of fully sequenced inbred lines). **b,** I161V frequency increases with increased pesticide use (linear mixed-effect model). **c,** I161V shows higher variance in frequency compared to matched control SNPs across populations (orange dashed line indicates I161V). **d,** Seasonal changes in I161V frequency at Linvilla Orchards showing decline from fall (dark blue) to spring (pink) samples during insecticide-free periods (turquoise, mid-fall to mid-spring) (generalized linear model, mean ± s.e.m.). **e,** Cumulative frequency changes at Linvilla Orchards samples show elevated allele frequency fluctuations of I161V compared to matched control SNPs (orange dashed line indicates I161V).

To test for the beneficial dominance reversal of the resistant *Ace* alleles, we used a laboratory-based approach to measure key fitness-associated phenotypes in organophosphate-rich and -free environments (**Fig. 2a,b**). Using the LNPA panel of inbred lines (**Extended Data Fig. 1a,b**), we took a round robin approach to generate recombinant populations with homozygous sensitive, homozygous resistant, and heterozygous genotypes for each resistant allele (S: IGFG, R1: VGFG, R2: VGFA, R3: VAYG) (see **Methods for details**). This approach[38] allowed us to control for the genotype at the *Ace* locus while allowing diversity in the rest of the genome, thus making more likely that associated phenotypic effects across recombinant populations are driven by the variation at *Ace* locus itself.

We first estimated resistance to organophosphates using malathion LD_{50} values (dose causing 50% egg-to-adult mortality). The resistance mutations alter the shape of AChE's active site, preventing malathion binding[5]. The R2 and R3 *Ace* alleles significantly increased malathion LD_{50} by ~5.8x and ~7.8x respectively ($p < 0.001$ for both), and were strongly dominant over the sensitive S *Ace* allele, with dominance *h* of 0.78 and 0.77 for R2 and R3, respectively ($p < 0.001$ for $h > 0.5$ in both cases). The R1 *Ace* allele showed no significant increase in malathion resistance ($p = 0.646$) with inconclusive dominance effects (p 0.751) (**Fig. 2, Extended Data Fig. 2, Extended Data Table 1**). We expected resistance to be dominant because malathion covalently binds to and inactivates the sensitive S *Ace* allele rendering it effectively loss-of-function, while the resistant *Ace* alleles remain functional. This pattern follows Wright's physiological theory of dominance[7], which predicts that functional alleles are dominant over loss-of-function alleles, as even one copy of the functional allele often provides sufficient gene activity to carry out the required function.

137 While these mutations provide resistance benefits, they also impair AChE activity and
138 stability[39], likely rendering them deleterious in the absence of insecticides[40]. We assessed the
139 cost of resistance in the absence of organophosphates by quantifying two key fitness-associated
140 phenotypes affected by impaired gene function: viability (egg to adult survival) and fecundity
141 (number of eggs laid by gravid females). All homozygous resistant genotypes exhibited lower
142 phenotypic fitness values compared to the homozygous sensitive genotype, for either or both of
143 these phenotypes, with viability reductions ranging from 12.4% to 16.9% (all $p < 0.001$) and
144 fecundity reductions from 16.2% (R2R2, $p = 0.37$) to 46.8% (R3R3, $p < 0.001$). The costs driven
145 by the three resistant alleles were either significantly recessive for at least one of the phenotypes
146 for the strongest resistance alleles R2 and R3 (viability R2: $h = 0.17$, $p = 0.027$, fecundity R3: h
147 = -0.02, $p = 0.001$), or indistinguishable from codominance for R1 (**Fig. 2g-l, Extended Data**
148 **Tables 2-3**). Overall, the sensitive S *Ace* allele is beneficial and dominant/codominant and never
149 recessive towards its resistant counterparts in terms of the costs in viability and fecundity in the
150 absence of malathion.

151 These results are consistent with the beneficial reversal of dominance. They also suggest
152 that the response to organophosphates at the concentrations similar to the LD_{50} of the sensitive
153 homozygous genotype should induce a very rapid increase in the frequency of the resistant *Ace*
154 alleles and in the level of overall resistance, given that resistant *Ace* alleles are strongly
155 beneficial and dominant. We also expect that after a reversal in selection pressure (removal of
156 insecticides), the trajectory of resistant alleles should depend on their starting frequency. When
157 initially rare, they should decline slowly due to their recessive costs hidden in heterozygotes.
158 When initially common, they should decline more rapidly as these recessive costs become
159 evident in homozygotes.

Figure 2

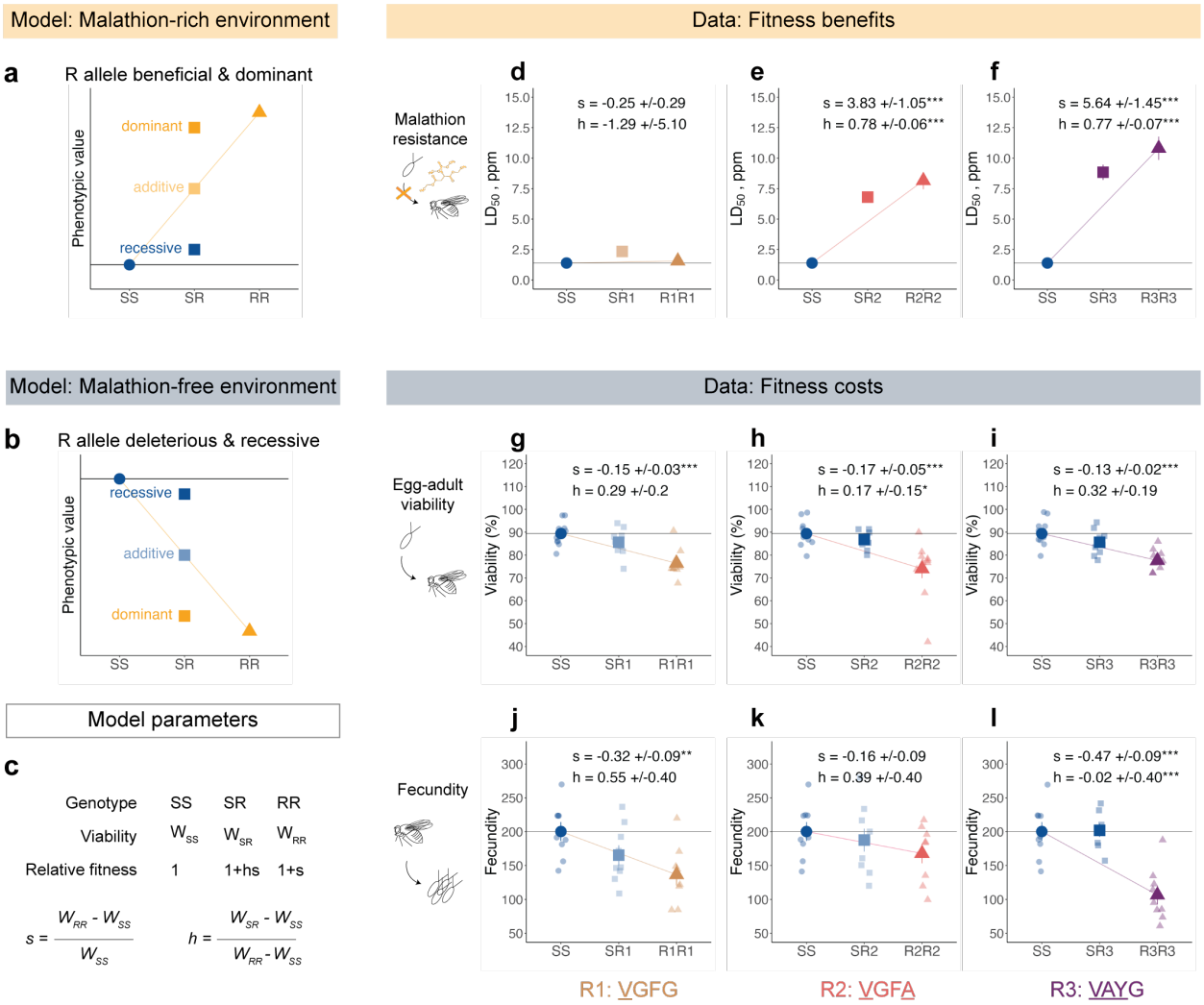

Figure 2. Beneficial reversal of dominance of organophosphate-resistant *Ace* alleles for fitness-associated phenotypes relevant to malathion-rich and malathion-free environments. **a-b**, Under the beneficial dominance reversal, R alleles should be beneficial and partially or completely dominant in malathion-rich environments ($W_{SR} > (W_{SS}+W_{RR})/2$, orange), and deleterious and partially or completely recessive in malathion-free environments ($W_{SR} < (W_{SS}+W_{RR})/2$, blue). **c,** Selection (s) and dominance (h) coefficients for each fitness-associated phenotype are estimated based on the viability selection model. If s>1, the resistant R *Ace* allele is beneficial; if s<1, it is deleterious. If h=1, the resistant R *Ace* allele is dominant to the sensitive S allele; if h=0, the reverse is true. **d-l**, Comparison of malathion LD_{50} (**d,e,f**), egg-adult viability (n=10 technical replicates, 50 eggs/replicate) (**g,h,i**), and fecundity (n=8–10 technical replicates, 5 females/bottle/3 days) (**j,k,l**) among *Ace* genotypes. Malathion LD_{50} was calculated from a four-parameter logistic model fitted to egg-adult viability measurements on media with a range of malathion concentrations (n=2 technical replicates, 50 eggs/replicate, see **Extended Data Fig. 2**). Egg-adult viability and fecundity data were analyzed with logistic and linear regression models.

161 To test these predictions, we directly investigated the population dynamics at the *Ace*
162 locus in an ecologically realistic environment by evolving replicate *D. melanogaster* populations
163 in the presence and absence of seasonally fluctuating malathion in field mesocosms at an
164 experimental orchard in Pennsylvania (**Fig. 3a,** see **Methods**). We established 20 replicate
165 populations derived from a baseline population constructed from the LNPA panel of 76 inbred
166 lines used in our lab experiments (**Extended Data Fig. 1**). These lines were outbred for 4
167 generations in large indoor cages before ~1000 males and females were used to seed each
168 outdoor cage (see **Methods**). After ~4 weeks of untreated propagation, we divided the
169 populations into ten malathion-treated and ten untreated outdoor cages. To mimic natural
170 insecticide exposure, we applied stepwise increasing concentrations of commercial malathion in
171 the growth media of the treated populations (1.5-2.5 ppm from July 21 to August 24, 2021,
172 followed by 7.5 ppm until September 6, 2021). These doses exert strong selection for resistant
173 *Ace* alleles based on our lab LD_{50} measurements (**Extended Data Fig. 2**). Following a reversal
174 of selection pressure (removal of malathion), the experiment continued without insecticides in all
175 20 cages through December 22, 2021. Throughout the experiment, we tracked population
176 dynamics, malathion resistance, and genome-wide allele frequencies at eight timepoints (~every
177 one to two generations), focusing on trajectories of resistant *Ace* alleles and linked sites in
178 response to fluctuating malathion treatment (**Fig. 3a**).

Figure 3

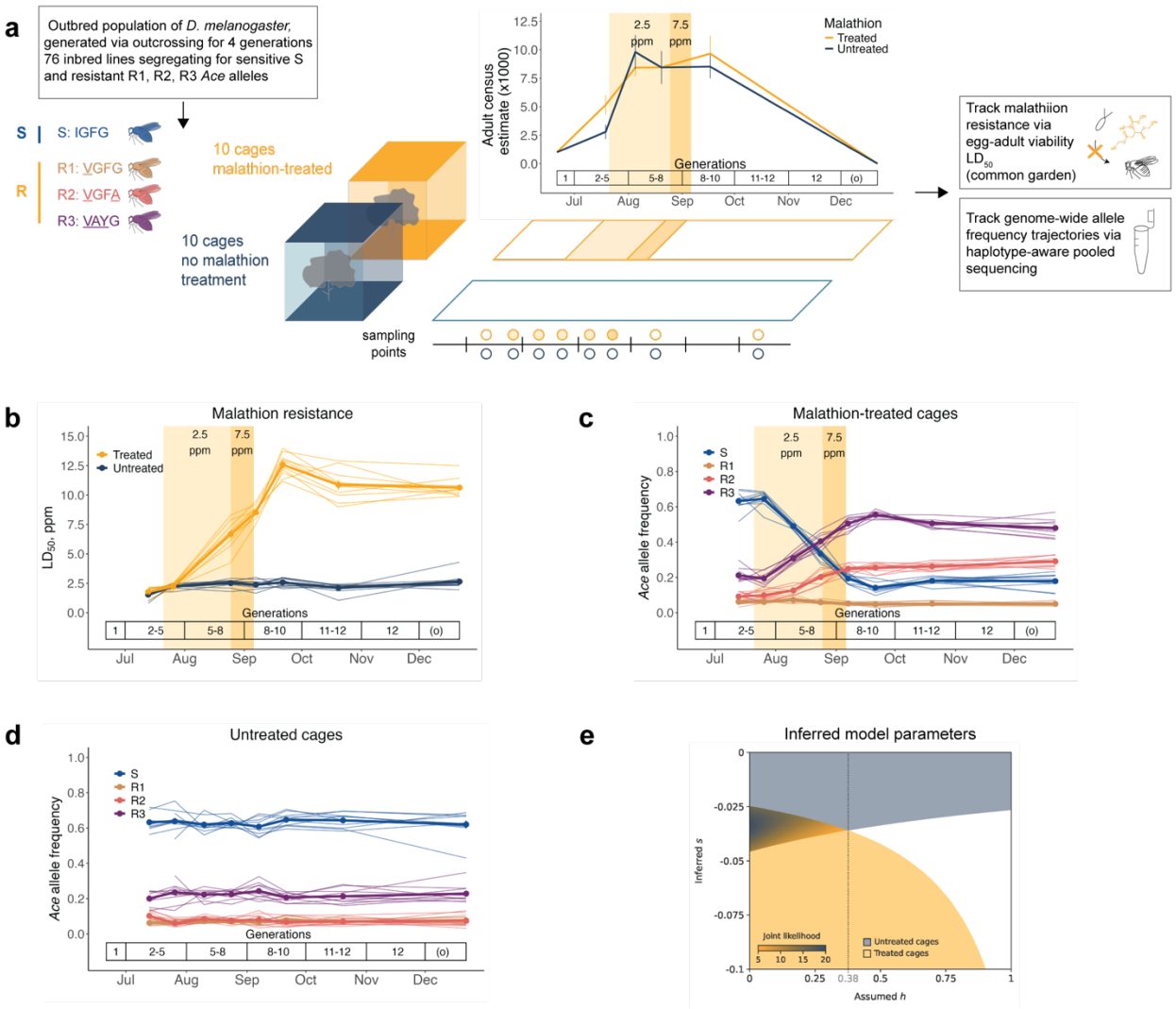

Figure 3. Beneficial reversal of dominance of resistant *Ace* alleles for fitness in an ecologically realistic environment. a, Twenty field mesocosm cages were seeded with an outbred population of *D. melanogaster* generated via outcrossing for 4 generations 76 inbred lines carrying the sensitive S and resistant R1, R2, and R3 Ace alleles. Ten cages received a malathion pulse after the initial population establishment. Eight timepoints were sampled to track the evolution of malathion resistance and genome-wide allele in the treated and untreated populations. Malathion did not affect estimated adult fly population sizes (mean ± s.e.m.) in treated populations. **b,** The malathion pulse led to a significant increase and subsequent decline of resistance (LD_{50}, ppm) in the treated populations while resistance remained stable in the untreated populations. For LD_{50} calculations see **Methods** and **Extended Data Fig. 3**. Light lines/points show individual populations (orange, treated; blue, untreated), dark lines/points represent mean ± s.e.m. (n=10 populations per treatment group). **c-d,** Trajectories of *Ace* alleles in treated (**c**) and untreated (**d**) populations. In treated populations, the malathion pulse led to a significant increase in the frequency of the resistant R2 and R3 *Ace* alleles, followed by a decline in the frequency of R3. *Ace* allele frequencies remained stable in the untreated populations. Light lines/points show individual allele trajectories, dark lines/points represent the mean ± s.e.m. (n = 10 populations per treatment group). (**continued on next page**)

Figure 3 (continued). e, Inferred selection (s) and dominance (h) coefficients from changes in the resistant *Ace* allele frequency. The colored ranges show the selection coefficients corresponding to the 0.95 confidence intervals of the slope distribution, obtained by bootstrapping cages within each treatment group. The overlap between the orange (treated cages) and dark blue (untreated cages) restricts the possible values of *s* and *h*. Within that overlap, lower values of *h* better explain both sets of data, as shown by higher values of the joint likelihood calculated from the bootstrap distributions (see **Methods**). All results of statistical tests can be found in **Extended Data Tables 4-6**.

The first surprising result was that the seasonal population dynamics were qualitatively similar in both malathion-treated and untreated cages (**Fig. 3a**). In all cages, population sizes increased through the summer months until reaching maximum size and then slowly declined in late Fall as abiotic conditions worsened. We interpret the unchanged seasonal population dynamics as an indication that population size in all cages is primarily limited by high levels of pre-adult mortality which masks the additional mortality imposed by malathion.

To characterize malathion resistance, we tracked egg to adult survival on diets with 0-15 ppm malathion and estimated LD_{50} at each timepoint per population (see **Methods** and **Extended Data Fig. 3**). In malathion-treated cages, resistance increased rapidly from ~2.2 ppm to ~12.6 ppm during treatment ($t = 24.26$, $p < 0.001$), followed by a significant decline to ~10.6 ppm after removal of malathion ($t = -3.96$, $p = 0.001$) (**Fig. 3b, Extended Data Table 4.1**). In contrast, resistance levels in untreated cages remained stable at ~2.2 ppm throughout the experiment ($t = 1.07$, $p = 0.288$) (**Fig. 3b, Extended Data Table 4.2**).

Using a haplotype-aware method to analyze pooled sequencing data[41], we inferred the frequency dynamics of the sensitive and resistant *Ace* alleles (see **Methods**). In treated cages, the resistant *Ace* alleles R2 and R3 increased significantly during malathion treatment (R2: $t = 13.93$, $p < 0.001$; R3: $t = 27.59$, $p < 0.001$) with the speed of change consistent with the selection coefficients (*hs*) on the order of 150-200% per generation, with R3 subsequently declining post-treatment ($t = -5.18$, $p < 0.001$) (**Fig. 3c, Extended Data Table 5**). The R1 allele did not increase significantly during the malathion phase, consistent with our lab data showing that it confers no

200 detectable malathion resistance (**Fig. 2c, Extended Data Table 5**). In untreated populations, all
201 resistant *Ace* allele frequencies did not show detectable change in frequency (**Fig. 3d, Extended**
202 **Data Table 6**).

203 To assess the contribution of the resistant *Ace* alleles to malathion resistance evolution in
204 the field mesocosms, we applied a viability selection model parametrized by lab-measured *Ace*
205 genotype viabilities (see **Methods**). This model closely recapitulated both the allele frequency
206 trajectories (**Extended Data Fig. 4a,b**) and the evolution of malathion resistance (**Extended**
207 **Data Fig. 4c,d**) observed in the field mesocosms. The agreement between model predictions and
208 experimental data provides compelling evidence that *Ace* is the major effect locus conferring
209 malathion resistance in the treated cages.

210 The results from the field mesocosms were qualitatively consistent with our expectations.
211 The *Ace* genetic system exhibited two key behaviors, rapid response to malathion treatment and
212 maintenance of resistance at low levels in its absence. In the malathion-treated cages, we
213 observed a significant decline of high-frequency resistant *Ace* alleles post malathion treatment,
214 indicating considerable fitness costs for resistant alleles when common. In contrast, untreated
215 cages showed fairly stable frequencies of low-frequency resistant alleles, suggesting low
216 selection coefficients (s) or dominance parameters (h) in the absence of malathion.

217 To obtain bounds on evolutionary parameters, we fit the allele frequency data of the
218 treated and untreated cages to a viability selection model where all resistant alleles share the
219 same fitness cost (see **Methods**). The model that fits both datasets best had low cost ($s \sim 2.5$ to
220 5%) and low dominance values ($h < 0.38$) (**Fig. 3e**). At higher values of h, there is no single
221 selection coefficient that can explain the patterns of allele frequency change for both treated and
222 untreated cages, and the likelihood of the data is higher the closer h is to zero. Overall, the data

223 are consistent with the fitness cost of organophosphate resistance being recessive and low,
224 allowing the resistant *Ace* alleles to persist at low frequencies for extended periods of time.
225 Such rapid frequency fluctuations of the *Ace* alleles are expected to affect variation at
226 linked genetic regions. The *Ace* genetic system presented us with a rare opportunity to study
227 these effects directly as the resistant alleles at the *Ace* locus are well-defined, the key resistant R2
228 and R3 *Ace* alleles increased in frequency during the malathion treatment and declined
229 afterwards, and the linkage patterns of genome-wide SNPs with the *Ace* alleles at the beginning
230 of the experiment are known from our inbred line genotypes. To characterize the extent of
231 forward and reverse sweeps driven by the R2 and R3 alleles during and after malathion
232 treatment, respectively, we used a two-step approach (see **Methods** for details). First, we
233 employed quasibinomial logistic regression to estimate genome-wide allele frequency changes
234 during malathion treatment (July 26 to September 21, 2021) and post-treatment (September 21 to
235 December 22, 2021). Next, we quantified changes in allele frequencies in SNPs tightly linked to
236 the sweeping R2 and R3 *Ace* alleles across the genome ($r^2 > 0.03$ and frequency > 60% in
237 resistant lines, *Ace*-linked) and those that were largely unlinked ($r^2 < 0.01$, control).
238 During the malathion treatment, we observed a virtually chromosome-wide forward
239 selective sweep driven by the R2 and R3 *Ace* resistant alleles in the malathion-treated
240 populations (**Fig. 4a**). This is consistent with the extremely rapid rise of the *Ace* alleles over 2-4
241 generations and the maximum recombination rate of ~5cM/Mbp in *D. melanogaster*, implying
242 the effects conservatively extending over a region of ~5-10 Mbp. The effect sizes of *Ace*-linked
243 sites were consistently elevated above the control sites across the chromosome arms 3L and 3R.
244 The sweep in the 3R chromosome was located from ~4Mbp to 17Mbp (~13Mbp wide), which
245 includes the *Ace* locus at 9.6Mb and extended to the 3L chromosome from ~5Mbp to 19Mbp

246 (~14Mbp wide). Note that, around position 19.5Mb on chromosome arm 3L control sites showed
247 a strong directional perturbation while *Ace*-linked sites uniformly decreased in frequency,
248 possibly suggesting the presence of an additional locus responding to malathion treatment that
249 interfered with the *Ace* sweep (**Fig. 4a,** asterisk**)**. Similarly, another putative locus was detected
250 on chromosome arm 2R, where both *Ace*-linked and control sites showed comparable frequency
251 perturbations (**Fig. 4a** asterisk). The study of these additional adaptive loci to malathion
252 treatment is beyond the scope of this work. As expected, in the untreated populations where the
253 frequencies of the R2 and R3 *Ace* alleles remained stable (**Fig. 3d**), *Ace*-linked sites showed no
254 elevated frequency changes compared to the control sites (**Fig. 4b**).

255 After the cessation of malathion treatment and the associated reversal of the insecticide
256 selection pressure, we detected an ~5Mbp reverse sweep driven by the R2 and R3 *Ace* alleles in
257 the malathion-treated populations (**Fig. 4c**). Individual SNPs within 1Mbp of the *Ace* locus
258 demonstrated a strong reversal effect, in which sites that increased in frequency during treatment
259 tended to decrease afterwards, with this reversal being significantly stronger for *Ace*-linked
260 compared to control sites (**Fig. 4e**). As expected, in the untreated populations, *Ace*-linked sites
261 showed neither significant median frequency changes (**Fig. 4d**) nor the reversal behavior (**Fig.
262 4f**). Of note, our ability to detect the reversal of individual SNPs is affected by the degradation of
263 the initial haplotype structure due to recombination through the course of the experiment, making
264 it possible that the extent of the reverse sweep is even longer than 5Mbp.

Figure 4

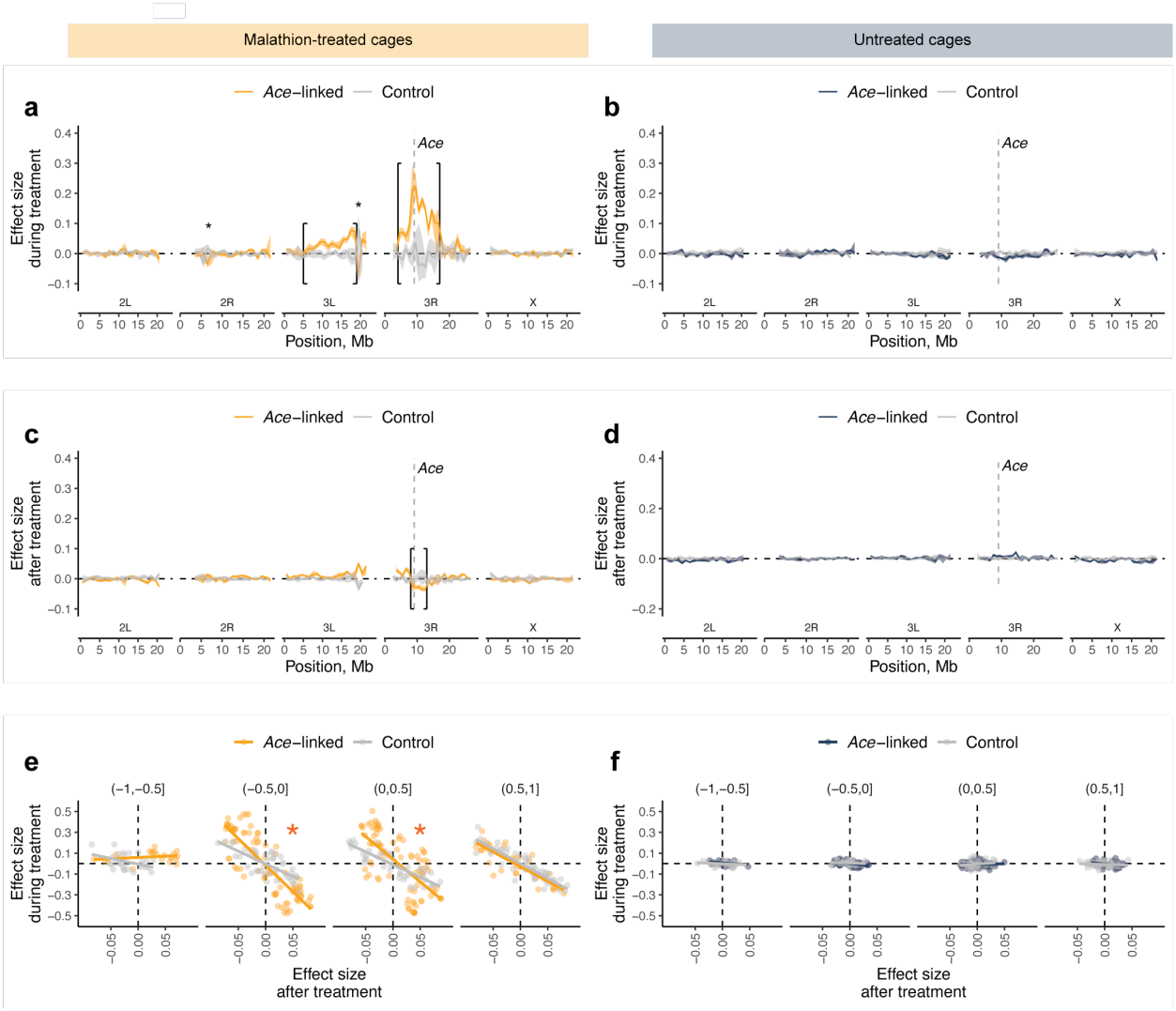

265

Figure 4. Strong fluctuating selection of resistant *Ace* alleles caused chromosome-scale forward sweep during malathion treatment and reverse sweep after treatment. **a-d**, Effect sizes (median allele frequency changes) for *Ace*-linked (orange/blue) and unlinked control (grey) SNPs in 1Mbp windows across the genome were estimated using quasibinomial logistic regression (see **Methods**). Changes during malathion treatment in treated (**a**) and untreated (**b**) populations. Changes after treatment cessation in treated (**c**) and untreated (**d**) populations. The brackets represent the inferred width of the sweep. Stars indicate additional adaptive loci to malathion treatment. **e-f**, Comparison of effect size for *Ace*-linked (orange/blue) and unlinked control (grey) SNPs during (y-axis) and after malathion treatment (x-axis) in malathion-treated (**e**) and untreated (**f**) populations within 1Mb from *Ace*. Each panel shows SNPs grouped by their distance from *Ace* (in Mb): [-1, -0.5], [-0.5, 0], [0, 0.5], and [0.5, 1]. In panel **e**, red stars indicate regions where the regression slopes significantly differ between *Ace*-linked and unlinked control SNPs.

266 Here we provide compelling evidence, both in the laboratory and in a highly replicated
267 field mesocosm experiment, for beneficial dominance reversal at a large-effect locus subject to
268 strong, temporally fluctuating selection. In the lab, we showed that resistant *Ace* alleles are
269 beneficial and dominant in the presence of organophosphates yet become deleterious and
270 recessive in their absence. Based on these results, we predicted the rapid increase in frequency of
271 the resistant *Ace* alleles in the presence of organophosphates and the relative stability in their
272 absence. The field mesocosm experiment together with modeling confirmed our predictions,
273 revealing that the cost of resistance is likely recessive, as only a recessive cost is consistent with
274 the observed stability when rare and the reduction in frequency when common. Critically, we
275 also demonstrate a way to quantify dominance in fitness in field mesocosms by measuring allele
276 trajectories under selection starting at different frequencies[4].
277 Our findings allow us to speculate about the likely mechanistic reasons and prevalence
278 for dominance reversals in fitness under temporally varying selection. In the presence of
279 organophosphates, the benefit of the resistant *Ace* allele should be dominant because the reduced
280 activity of the sensitive *Ace* allele will be compensated by the sufficient activity of the resistant
281 *Ace* allele. This follows Wright's physiological theory of dominance[7] which posits that reduction
282 in gene activity by one half should have only a modest fitness effect for large-effect loci due to a
283 concave mapping of gene activity to fitness. Similarly, in the absence of organophosphates, the
284 cost should be recessive because the sensitive *Ace* allele maintains normal function and the logic
285 of the physiological model of dominance applies again. This reversal of dominance therefore
286 extends Wright's model of dominance as the identity of the loss-of-function, deleterious and
287 recessive allele shifts in concert with the fluctuating environment. This mechanism is compatible
288 with the stochastic additive scale and concave fitness function (SAS-CFF) model which predicts

289 the maintenance of polymorphisms in variable environments[42]. We argue that such reversals of
290 dominance should be widespread for polymorphic large-effect loci under temporally varying
291 selection in nature. For example, large-effect loci involved in resistance to insecticides and host
292 plant toxins, both of which are subject to temporally varying selection, likely exhibit similar
293 dominance patterns[43,44].

294 An important implication of fluctuating selection affecting large-effect loci is the effect
295 on linked genomic variation. Our experimental evolution setup allowed us to quantify a
296 chromosome-wide forward sweep and a reverse sweep at the *Ace* locus in response to fluctuating
297 insecticide selection. These perturbations are very hard to detect without knowing the exact
298 linkage structure genome-wide, as such old alleles are present on diverse genetic backgrounds.
299 Given the data that *D. melanogaster* genome contains a fair number (tens to hundreds) of large-
300 effect alleles displaying large frequency shifts due to fluctuating selection[14,15] and the likelihood
301 that this is the case for many other species[18,19], fluctuating selection at large-effect loci could act
302 as a major force shaping levels of genetic variation in natural populations[28,29].

303 To conclude, our work demonstrates that beneficial reversal of dominance can operate at
304 large-effect loci, stabilizing a large effect functional polymorphism and enabling rapid responses
305 to environmental change. To test the generality of this mechanism, future studies should examine
306 other genetic systems, particularly large-effect loci with known genetic architecture responding
307 to temporally varying environments, such as those conferring resistance to host plant toxins and
308 pesticides. Determining the biochemical basis of dominance reversal in these systems would test
309 our proposed extension of Wright's physiological theory. Additionally, investigating the effects
310 of repeated fluctuating selection cycles could reveal how recurrent forward and reverse sweeps

311 shape genome-wide variation patterns, potentially illuminating a key evolutionary force driving

312 genomic variation in natural populations across taxa.

Acknowledgements This project was supported by grants from the National Institute of General Medical Sciences of the National Institutes of Health (Award number 1K99GM143455-01 to M.K, Grant 5R01GM100366-08 and 5R01GM137430-02 to P.S., Award Number 5R35GM118165-07 to D.A.P), the Sarah Hotchkis Ketterer Graduate Fellowship from Stanford University (to A.S.L.), the National Science Foundation (Grant PRFB 2109407 to M.C.B.), and the Stanford Biology Summer Undergraduate Research Program (to Z.K.M. and A.H.). The authors thank Marcus Feldman for helpful discussions and assistance with modeling *Ace* allele frequency evolution, Danae Papadopetraki for assistance with statistical analyses of the phenotypic and genomic data, Axel Wiberg for feedback on statistical analyses of the genomic data, Emily Behrman for feedback on the day degree model for generation estimation, Jessica Rhodes for helpful discussions and assistance with statistical analyses of the DEST data, and Anastasia Andreeva for assistance with phenotyping. The authors are very grateful to Jean Villa, Jessica Rhodes, Meike Wittmann, Noah Whiteman, and Marcus Feldman for feedback that improved the earlier versions of the manuscript.

Author Contributions M.K was responsible for conceptualization, investigation, formal analysis, writing original draft, writing-review and editing, visualization, and funding acquisition; A.L. was responsible for formal analysis, visualization, and writing-review and editing; M.B. was responsible for formal analysis and investigation; E.L. was responsible for formal analysis, visualization, and writing-review and editing; S.G. was responsible for formal analysis; A.H., CT, and Z.K.M. were responsible for investigation; P.S. and D.A.P. jointly supervised the research. P.S. was responsible for conceptualization, investigation, formal analysis, writing-review and editing, and funding acquisition. D.A.P. was responsible for conceptualization, investigation, formal analysis, writing-review and editing, and funding acquisition.

Methods

Population genomic analysis for variation of organophosphate-resistant *Ace* alleles across space and time

We first conducted a literature review to compile all known naturally segregating target site resistance mutations in the acetylcholinesterase (*Ace* gene) protein of *D. melanogaster* that confer resistance to organophosphates. Mutero and colleagues in 1994[45] first identified the resistance mutations F115S, I199V, I199T, G303A and F368Y, and numbered them based on the precursor acetylcholinesterase (AChE) protein. Menozzi and colleagues in 2004[5] identified combinations of the resistance mutations I161(199)V, G265(303)A, F330(368)Y and G368(406)A in worldwide organophosphate-resistant *D. melanogaster* strains and numbered them based on the mature AChE protein (numbers in the brackets refer to the precursor AChE protein). They did not identify the resistance mutation F77(115)S. At position 77, the mutation TTC to T**C**C changes phenylalanine to serine (Chr3R: 9,070,101, v5.39). At position 161, the mutation ATC to **G**TC changes the isoleucine to valine (Chr3R:9,069,721, v5.39). At position 265, the mutation GGC to G**C**C changes the glycine to alanine (Chr3R:9,069,408 , v5.39). At position 330, the mutation TTT to T**A**T changes the phenylalanine to tyrosine (Chr3R:9,069,054 , v5.39). At position 368, the mutation GGC to G**C**C/G**CT** changes the glycine to alanine (Chr3R: 9,063,921 , v5.39). The AChE protein's numbering changed between the studies after its crystallization in 2000, which defined the N-terminal signal peptide and the C-terminal sequence[46]. The mutation G368A was missanotated in the study of adaptation of *D. melanogaster* to organophosphate insecticides by Karasov and colleagues[6].

<u>Organophosphate-resistant *Ace* alleles in DGRP and LNPA inbred lines</u>

361 We characterized the presence of organophosphate-resistant *Ace* alleles in two fully
362 sequenced inbred line panels, the Drosophila Genetic Reference Panel (DGRP) and our LNPA
363 panel of inbred lines. The DGRP panel consists of 205 inbred lines derived from wild-caught
364 females collected at the Raleigh, North Carolina Farmers Market in 2003[37]. The LNPA panel
365 consists of 76 inbred lines derived from wild-caught individuals collected in Spring and Fall
366 from Linvilla Orchards, Media PA USA[14]. Both panels contain the two common resistant *Ace*
367 alleles (Ace-R1: VGFG and Ace-R3: VAYG) at high frequency, the sensitive *Ace* allele (Ace-S:
368 IGFG), and other rare resistant alleles. The LNPA panel also contains the resistant *Ace* allele
369 Ace-R2: VGFA at high frequency. We used the LNPA panel for our lab and field mesocosm
370 experiments.
371
372 Spatial and seasonal variation of organophosphate-resistant *Ace* alleles in natural *Drosophila*
373 *melanogaster* populations
374 To examine the spatial variation of the I161V polymorphism, a marker of common
375 organophosphate-resistant *Ace* alleles (Ace-R1: VGFG, Ace-R2: VGFA, Ace-R3: VAYG), we
376 first analyzed the relationship between country-level pesticide use and I161V frequency in
377 *Drosophila melanogaster* populations. We obtained pesticide use data from the Food and
378 Agriculture Organization (FAO) FAOSTAT database[36], which provides country-level estimates
379 of pesticide use per area of cropland. For population genomic data, we used the Drosophila
380 Evolution over Space and Time (DEST) database, which contains pooled genome-wide allele
381 frequency estimates from 753 population samples of *D. melanogaster* collected worldwide. For
382 our analyses, we included pesticide use data and genomic data for the period of 2000-2022.

383 To visualize the spatial distribution of insecticide use and frequency of the I161V
384 polymorphism across locations, we created a choropleth map where countries are shaded based
385 on their pesticide use per cropland area, with pie charts indicating the frequency of the resistant
386 (I161V) and sensitive alleles at sampled locations. For each location, we calculated median allele
387 frequencies across available samples for the period 2000-2022. To test whether insecticide use
388 predicts the frequency of the resistance allele I161V, we fitted a linear mixed effects model using
389 the lmer() function in the R package lme4 (version 1.1.33). The model included I161V frequency
390 as the response variable and insecticide use per cropland area as a fixed effect. We included a
391 random effect for cities.

392 In addition, to further test whether I161V shows evidence of spatial selection rather than
393 drift, we compared its variance across samples collected in spring to matched control SNPs. We
394 selected control SNPs based on three criteria: (1) located within 2Mb but at least 100kb away
395 from *Ace* to avoid linked SNPs, (2) within the ln(3R)K cosmopolitan inversion to match
396 inversion status, and (3) average frequency across samples within 4% of the median frequency of
397 the I161V resistance mutation. We used the cumulative distribution function (CDF) to quantify
398 how extreme the I161V variance was compared to the control SNPs.

399 To examine the temporal variation of the I161V polymorphism, we first tested two
400 hypotheses: (1) whether the frequency of the resistant allele decreases during winter months
401 when insecticide pressure is relaxed, potentially due to fitness costs, and (2) whether the
402 frequency of the resistant allele increases during the growing seasons when insecticides are
403 applied. We analyzed time series data from Linvilla Orchards, a non-organic orchard in
404 Pennsylvania, USA. Samples were collected near apple trees from 2009 to 2015, with paired
405 spring and fall collections each year, allowing us to test both hypotheses. To account for

406 sampling variance in pooled sequencing data, we calculated the effective number of
407 chromosomes sampled (Nc) following Machado et al. (2016), where Nc = (1/N + 1/R)^(-1), with
408 N being the number of chromosomes in the pool (2 × number of flies) and R the read depth at the
409 site. We then tested for systematic seasonal changes using generalized linear models (GLM) with
410 binomial error structure. The models used the number of resistant and susceptible alleles
411 (weighted by Nc) as the response variable and season as a categorical predictor. For the winter
412 decline hypothesis, we paired each fall sample with the following spring sample. For the summer
413 increase hypothesis, we paired each spring sample with the following fall sample from the same
414 year. This approach allowed us to directly test for consistent directional changes in allele
415 frequencies across seasons while accounting for both biological and technical sources of variance
416 in the data.

417 Finally, to test whether the temporal dynamics of I161V reflect selection rather than drift,
418 we compared its frequency fluctuations to those of matched control SNPs at Linvilla. To
419 quantify temporal variation, we calculated the cumulative absolute change in I161V allele
420 frequency over time as the sum of frequency differences between consecutive timepoints. This
421 metric captures the total magnitude of frequency changes, regardless of direction. We selected
422 control SNPs that had similar starting conditions as I161V, with initial frequencies matching the
423 I161V frequency (0.42) at the first Linvilla timepoint within ±4%. To ensure a valid comparison,
424 control SNPs were selected from within the same genomic region and inversion status as I161V,
425 while excluding potentially linked sites (same criteria as for the spatial analysis). We then used
426 the cumulative distribution function to assess whether I161V's temporal variation was
427 significantly greater than that observed in the matched control SNPs, which would suggest that
428 its frequency changes are driven by seasonal selection rather than drift.

429

430 **Laboratory experiments to estimate the dominance of resistant *Ace* alleles for fitness-**
431 **associated phenotypes in the presence and absence of malathion**

432 To assess whether the dominance of each resistant *Ace* allele (Ace-R1: VGFG, Ace-R2: VGFA,
433 Ace-R3: VAYG) over their sensitive counterpart (Ace-S: IGFG) reverses for fitness-associated
434 phenotypes that are primarily under selection in organophosphate-rich and -free environments,
435 we first used our LNPA panel of inbred lines to generate recombinant populations with
436 homozygous sensitive, homozygous resistant, and heterozygous *Ace* genotypes for each *Ace*
437 allele. This step was meant to bring potential deleterious, recessive mutations in the inbred lines
438 into heterozygosity. We then measured malathion resistance, viability and fecundity in
439 homozygous and heterozygous populations for each *Ace* genotype.

440

441 Generation of recombinant populations with homozygous sensitive, homozygous resistant, and
442 heterozygous *Ace* genotypes

443 To generate recombinant populations for each *Ace* allele, we first intercrossed 2-3 inbred
444 lines with the same *Ace* allele using a round robin cross scheme (e.g., Line_1 SS x Line_2 SS,
445 Line_2 SS x Line_3 SS, Line_3 SS x Line_1 SS) to bring all founders with the same *Ace* allele
446 together (10 non-mated females x 10 males per round robin cross). We then combined 16 F1
447 flies (8 non-mated females and 8 males) from each of the round robin crosses per *Ace* allele to
448 establish the next generation. Subsequently, we maintained the homozygous populations in vials
449 and allowed them to recombine for four generations until we performed the phenotype
450 measurements. We used lines 12LN6-70_(B33), 12LN6-92_(B3), LNPA-3 for the sensitive *Ace*
451 allele (Ace-S: IGFG), lines 12LN6-86_(B29) and LNPA-53 for the R1 resistant *Ace* allele (Ace-

452 R1: VGFG), lines LNPA-14, LNPA-17 and LNPA-87 for the R2 resistant *Ace* allele (Ace-R2:
453 VGFA), and lines 12LN6-45_(B26), 12LN6-82_(B4), and 12LN6-94_(B19) for the R3 resistant
454 *Ace* allele (Ace-R3: VAYG).
455
456 Measurements of fitness-associated phenotypes
457 For all experiments, we first set up breeding cages with ~ 500 4-to-7-day-old flies of
458 homozygous or heterozygous populations for the sensitive and the resistant *Ace* alleles. To
459 generate the heterozygous recombinant populations, we crossed SS non-mated females with
460 homozygous males of each resistant allele (R1R1, R2R2, R3R3).
461 To compare the level of malathion resistance among the different alleles, we measured
462 egg-to-adult viability on diets that ranged in malathion concentration from 0 ppm to 30 ppm. For
463 this, we collected eggs of each population that were laid within a period of 24 hours and then
464 introduced 50 eggs of each population into narrow vials containing approximately 7 ml of
465 *Drosophila* growth media supplemented with the respective malathion concentration. We tested
466 each of the malathion concentrations in duplicate vials. We used commercial malathion of 50%
467 strength (Southern Ag Malathion 50% E.C.) and dissolved it in the *Drosophila* growth media.
468 This medium was kept overnight at 4ºC and used the next day for the assay. We monitored adult
469 eclosion every evening over a period of 10 days until all adult flies had enclosed.
470 To compare viability among the different genotypes, we introduced 50 eggs of each
471 population into narrow vials containing ~7 ml of *Drosophila* growth media. Each of the
472 genotypes were tested in 10 replicate vials. We monitored adult eclosion every evening over a
473 period of 7 days until all adult flies had enclosed.

To compare fecundity among the different genotypes, we used density-controlled (~50 eggs/vial) adult female progeny of each population. We introduced five 3-day-old females of each genotype in egg-laying bottles fitted with egg-laying caps filled with Drosophila growth media. Each day over a period of 3 days we counted the number of eggs laid. Each of the genotypes were tested in 8-10 replicate egg-laying bottles. The egg-laying caps were examined under a stereoscope where we counted the eggs laid each day over the 3-day period.

Statistical analysis of fitness-associated phenotypes

We assessed fecundity, viability, and malathion resistance for the three genotypes (SS, SR, RR) of each *Ace* allele (R1, R2, R3) using R (version 4.2.2). For fecundity and viability, we fitted linear and logistic regression models, respectively, calculating estimated marginal means and performing pairwise comparisons adjusted for multiple testing using the Benjamini-Hochberg procedure. We then implemented a bootstrap procedure (1,000 resamples) to estimate deviation from additivity, selection coefficient, and dominance coefficient. The deviation from additivity was calculated as W[SR] - (W[SS] + W[RR]) / 2, where W represents fitness (fecundity or viability) for each genotype. The selection coefficient *s* was computed as (W[RR] – W[SS]) / W[SS], indicating the relative fitness of the resistant genotype compared to the sensitive genotype. The dominance coefficient *h* was calculated as (W[SR] – W[SS]) / (W[RR] – W[SS]), measuring the degree to which the heterozygote phenotype is closer to either homozygote. Significance was assessed by testing whether results differed from zero (additivity and selection) or 0.5 (dominance). For malathion resistance, we estimated LD_{50} values for each genotype using four-parameter logistic dose-response models f(x) = c + (d-c) / (1 + e^(b(x-e))), where e is LD_{50}, d (upper limit) = 100%, c (lower limit) = 0%, and b is the relative slope around

497 e. For this, we used the L.4() function in the drc package (version 3.0.1)[47] in R (version 4.2.2)
498 with egg to adult viability at the range of malathion concentrations as the response variable. We
499 then used a bootstrap procedure (1,000 resamples) to compare LD_{50} values between genotypes
500 and calculate the same coefficients, substituting LD_{50} values for W in the formulas. For all
501 analyses, bootstrap resampling was used to calculate confidence intervals and p-values, with
502 significance assessed against null hypotheses of 0 (additivity and selection) and 0.5 (dominance).
503

504 **Field mesocosm experiments to track the evolution of malathion resistance and genome-**
505 **wide allele frequencies in the presence and absence of fluctuating malathion selection**
506

507 Experimental orchard and field mesocosm cages

508 To mimic the natural surroundings and weather conditions that flies are exposed to in nature, we
509 conducted the study in an experimental orchard at the University of Pennsylvania in
510 Philadelphia. The orchard consisted of cleared land with walk-in mesocosm cages (2m x 2m x
511 2m) constructed of fine mesh and built around metal frames (BioQuip PO 1406C). We planted a
512 dwarf peach tree in each mesocosm cage to provide flies with shade. All peaches were removed
513 before ripening to prevent flies from feeding or laying eggs on them. To provide flies with a
514 feeding and breeding substrate, we added 1.5lb aluminum loaf pans with 400ml Drosophila
515 growth media every two days during the experiment. To avoid an overcrowded developmental
516 environment for the eggs, each loaf pan was covered with a screen mesh lid every two days
517 during the experiment, and eggs were allowed to develop until eclosion ceased, at which point
518 adult flies were released into the general population. The loaf pans were placed on a shelving
519 unit oriented away from direct sunlight to protect them from rain and direct sun.

520

521 Establishment of experimental *D. melanogaster* populations in field mesocosm cages

522 To construct the baseline *D. melanogaster* population for the experiment, we crossed the
523 76 fully sequenced LNPA inbred lines from Pennsylvania. We used inbred lines to facilitate the
524 use of haplotype inference to attain high effective sequencing coverage[41]. To initiate the baseline
525 population, we combined 10 females and 10 males from each line into a single breeding cage.
526 After 4 generations of mating and density-controlled rearing in laboratory conditions, we
527 introduced 500 females and 500 males of a single age cohort into each mesocosm cage on June
528 21, 2021.

529

530 Malathion treatment over the course of the experiment

531 A diagram of the experimental design is shown in **Fig. 3a**. In the first step (*Establishment*
532 *phase*: June 21 to July 20, 2021), we established 20 replicate populations in mesocosm cages and
533 allowed them to expand in the absence of interventions. After establishment, the populations
534 were split into ten malathion-treated and ten malathion-untreated populations. To mimic the
535 insecticide exposure of flies in nature, the malathion-treated populations were exposed to
536 malathion in the summer. In nature, insecticides are mainly applied during summer for pest
537 control and their application ceases in the fall[48]. During the malathion treatment phase of the
538 experiment, we sequentially exposed the populations to stepwise increasing concentrations of
539 malathion, from 1.5 (July 21 to July 27, 2021) to 2.5ppm (July 28 to August 24, 2021) and
540 7.5ppm (August 25 to September 6, 2021). We used commercially available malathion grade of
541 50% strength (Southern Ag Malathion 50% E.C.) and dissolved it in the *Drosophila* growth
542 media. We selected malathion doses based on the Malathion 50% E.C. label instructions to

543 control small insect pests in the field and a previous long-term selection experiment for
544 malathion resistance in *D. melanogaster*[49]. The medium supplemented with malathion was
545 cooked once per week and stored at 4˚C until deployed. After the malathion treatment, the
546 experiment lasted until early winter (September 7 to December 22, 2021). Over the course of the
547 experiment, we performed high-resolution temporal sampling (~ bi-weekly sampling during the
548 summer and monthly during the fall) to track evolution of malathion resistance and genome-wide
549 allele frequencies.
550

551 **Tracking population size in the field mesocosms**

552 To make relative comparisons of population sizes between the malathion-treated and untreated
553 cages, we photographed 4 equal-size quadrats of the ceiling in each cage at dusk (approximately
554 2.5% of the ceiling for each quadrat). To count the number of adult flies in each photograph, we
555 designed and validated an algorithm for semi-automated image processing. The number of adult
556 flies in each of the 4 photographs was multiplied by 40 to correct for total surface area and obtain
557 4 population size estimates per cage.
558

559 <u>Statistical analysis of population data</u>

560 To assess the effects of time and malathion treatment on population size, we fitted a linear
561 mixed-effect model with the estimated population size as the response variable. We defined our
562 model to investigate the quadratic relationship of time with population size and to account for the
563 random effects attributable to differences in cages. The regression analysis was performed in R
564 (version 4.2.2) using lme4 (version 1.1.33).
565

566 **Tracking malathion resistance in the field mesocosms**

567 To characterize the rate and direction of the evolution of malathion resistance in the malathion-
568 treated and untreated populations, we repeatedly assayed the evolving populations. Prior to the
569 malathion resistance assay, we collected F1 eggs from each mesocosm cage and transferred them
570 in 2 groups of 200 eggs to bottles with media (i.e., density controlled) in a constant common
571 garden environment (25˚C, 12L:12D, 50% humidity) in the laboratory to distinguish evolution
572 from phenotypic plasticity. We then performed the malathion resistance assay with density and
573 age-controlled individuals from each mesocosm cage in the F2 generation (25˚C, 12L:12D, 50%
574 humidity). The common garden experiment for assaying malathion resistance took place at
575 Stanford University with F1 eggs in bottles with media shipped overnight from the University of
576 Pennsylvania.

577

578 Malathion resistance measurements

579 To characterize the level of malathion resistance in the malathion-treated and untreated
580 populations, we tracked egg to adult survival in the F2 generation on diets that ranged in
581 malathion concentration from 0 ppm to 15 ppm over the course of the experiment. For the
582 collection of F2 eggs, we placed ~ 400 4-to-7-day-old F1 individuals in breeding cages with egg
583 lay caps for 5-7 hours. We then introduced 50 F2 eggs in a narrow vial containing ~7ml of
584 *Drosophila* growth media supplemented with malathion. We tested each of the malathion
585 concentrations in duplicate vials. We used commercial malathion of 50% strength (Southern Ag
586 Malathion 50% E.C.) and dissolved it in the *Drosophila* growth media. This medium was kept
587 overnight at 4ºC and used the next day for the assay. We monitored adult eclosion every evening
588 over a period of 10 days until all adult flies had eclosed.

589

590 Statistical analysis of malathion resistance data

591 To assess the temporal dynamics of malathion resistance in both malathion-treated and untreated
592 cages, we fitted separate linear mixed-effects models using the lmer() function in the R package
593 lme4 (version 1.1.33). The response variable in these models was malathion resistance, measured
594 as the LD_{50} value, the dose that causes 50% egg-to-adult mortality. For the malathion-treated
595 cages, we modeled resistance changes over two distinct time periods: (1) from July 26, 2021, to
596 September 21, 2021, when populations were evolving under malathion treatment, and (2) from
597 September 21, 2021, to December 22, 2021, after malathion treatment had ceased. In contrast,
598 for the malathion-untreated cages, we assessed resistance changes over the full experimental
599 period, from July 26, 2021, to December 22, 2021. To avoid biases, we excluded data from July
600 13, 2021, because the LD_{50} estimate from this time point was underestimated due to a technical
601 error. In each model, we included time point as fixed effect, while a random intercept was
602 included for each cage to account for between-cage variability. The main outcome measure of
603 malathion resistance for each cage at each time point was the mean of 1–2 technical replicate
604 LD_{50} measurements. To estimate LD_{50} for each technical replicate per cage per time point, we
605 fitted four-parameter logistic dose-response models using the L.4() function in the drc package
606 (version 3.0.1) in R (version 4.2.2) with egg to adult viability at the range of malathion
607 concentrations as the response variable.

608

609 **Track genome-wide allele frequencies in the field mesocosms over time**

610

611 To track the trajectories of the resistant and sensitive *Ace* alleles and characterize the extent of
612 the sweep caused by the *Ace* alleles, we tracked genome-wide allele frequencies of the evolving

613 populations across the experiment using the software tool HAF-pipe. HAF-pipe estimates
614 genome-wide allele frequencies in the evolving populations via inference of known founder
615 haplotypes from low-coverage pooled sequencing data [41]. As part of our experimental design, we
616 performed whole-genome, low-coverage pooled sequencing of 100 randomly selected F1
617 females from each of the 20 evolving populations at eight time points through the experiment. To
618 measure biological and technical variation, we performed whole-genome, low-coverage pooled
619 sequencing of different sets of 100 randomly selected F1 females from the 20 evolving
620 populations at two time points collected at Stanford (biological replicates) and of same samples
621 of 100 randomly selected F1 females but processed independently (technical replicates). Last, to
622 evaluate the accuracy of HAF-pipe, we performed whole-genome, high-coverage pooled
623 sequencing of four biological replicate samples from the baseline population and for the evolving
624 populations at an early and a late time point. The data for the untreated cages were also used for
625 a recent independent study from Bitter and colleagues [15].
626
627 Sample collection, DNA extraction, library preparation, and sequencing
628 We collected samples from each population approximately every two generations during
629 the summer phase and every generation during the fall phase. To collect the samples, we placed a
630 new loaf pan with Drosophila growth media in each mesocosm cage one day before collection.
631 The next day, we transferred five groups of 200 F1 eggs to bottles with media, where we
632 controlled the density and maintained them in a constant laboratory environment of 25°C,
633 12L:12D, and 50% humidity. Three bottles with F1 eggs were kept at UPenn and two bottles
634 with F1 eggs were shipped overnight to Stanford. At Stanford, F1 adults were allowed to lay
635 eggs, and 200 F2 eggs were placed in vials for density control. For both the F1 and F2

636 generation, we harvested 4-to-7-day-old individuals after eclosion and preserved them in 100%
637 ethanol in 1.5ml vials at -20°C until further processing.
638 For each sample, we prepared genomic DNA from pools of 100 ethanol-preserved
639 females. We first submerged the samples twice in a rehydration buffer (400 mM NaCl, 20 mM
640 Tris-HCl pH 8.0, 30 mM EDTA) for 15 min at room temperature and then isolated genomic
641 DNA using the Monarch Genomic DNA purification kit (Cat No. 3010L, New England Biolabs).
642 The manufacturer's protocol was modified to include a step for tissue homogenization with two
643 3mm glass beads (Cat No. 11-312C, Fisher Scientific) in a bead beater for five minutes to ensure
644 complete homogenization of the flies so that the genomic DNA from each fly was equally
645 represented in the genomic DNA pool. We quantified the genomic DNA using the Qubit dsDNA
646 BR (Broad-Range) Assay kit (Cat No. Q32853, Life Technologies) on a Qubit
647 spectrophotometer and estimated its purity on a NanoDrop spectrophotometer.
648 We then prepared sequencing libraries using the Illumina DNA prep, (M) Tagmentation
649 kit (Cat No. 20018705, Illumina Inc.) and the Illumina UD Indexes sets (Cat No 20027123,
650 20027214, 20042666, 20042667, Illumina Inc.) for unique dual indexing. We modified the
651 manufacturer's protocol by preparing libraries in 1/5 of the recommended reaction volume to
652 maximize kit efficiency and pooling equimolarly amplified libraries in sets of eight after the
653 library amplification step. After the cleanup, we quantified the pooled libraries using a Qubit
654 spectrophotometer and an Agilent Bioanalyzer. Finally, the pooled libraries were 150bp paired-
655 end sequenced on the NovaSeq 6000 S2 platform at the Sequencing Service Center at the
656 Stanford Genomics Center and on a NovaSeq 6000 SP platform at Admera. All sequences will
657 be deposited in SRA.
658

659 Processing of DNA sequencing data for genome-wide allele frequency estimation

660 We trimmed the raw sequencing reads of adapter sequences and bases with quality score
661 < 20. We then mapped the trimmed reads to the *D. melanogaster* reference genome (v5.39) using
662 bwa and default parameters [50], and aligned reads were deduplicated using Picard tools. We
663 randomly sampled reads from the aligned bams to obtain an equivalent, genome-wide coverage
664 of 8x across all samples. We computed haplotype-derived allele frequency (HAF) estimates
665 using HAF pipe. Briefly, after using an expectation-maximization algorithm to estimate
666 haplotype frequencies in overlapping genomic windows from mapped sequence reads (originally
667 developed by Kessner and colleagues [51]) at each site previously identified as polymorphic in the
668 inbred reference panel, we summed the estimated frequencies of haplotypes carrying the
669 alternate allele to obtain HAFs . We conducted haplotype inference in window sizes that varied
670 proportionally to the expected length of un-recombined haplotype blocks, which varied as a
671 function of the estimated number of generations since the original outbreeding. HAFs were
672 compiled to only include those sites with an average minor allele frequency (MAF) > 0.02 in the
673 baseline population, and present in at least one evolved sample at a MAF > 0.01.

674

675 **Track trajectories of sensitive and resistant *Ace* alleles in the evolving populations over**
676 **time**

677

678 We first estimated the frequency of each of the 76 founder haplotypes in the *Ace* region
679 (Chr3R:9,063,921-9,069,721) in each of the malathion-treated and malathion-untreated
680 populations at each time point, focusing on the founders containing the four known resistance
681 mutations . To obtain an accurate measure of the frequency of each haplotype, we calculated the

682 mean frequency across the 10 overlapping genomic windows that included each site within the
683 region of interest.
684 We then estimated the relative frequency of each *Ace* allele, defined by the combination
685 of the four known resistance mutations, in each population at each time point. Given our
686 knowledge of the resistance mutation combinations for each founder, we computed the relative
687 frequency of each *Ace* allele (Ace-S: IGFG, Ace-R1: VGFG, Ace-R2: VGFA, Ace-R3: VAYG,
688 Ace-R4:IGFA, Ace-R5:IGYG, Ace-R6:VAFG, Ace-R7: VAYA) by summing the frequencies of
689 the haplotype blocks from the 76 founders that shared the same *Ace* allele. For founders
690 heterozygous for the *Ace* alleles, we divided the contributions of their haplotype block evenly
691 between the two corresponding *Ace* allele frequencies. *Ace* alleles with a frequency < 0.01%
692 (Ace-R4:IGFA, Ace-R5:IGYG, Ace-R6:VAFG, Ace-R7: VAYA) in the evolving populations
693 were excluded from further analysis.
694
695 Statistical analysis of *Ace* allele frequency data
696 To assess the temporal dynamics of *Ace* allele frequencies (Ace-S: IGFG, Ace-R1:
697 VGFG, Ace-R2: VGFA, Ace-R3: VAYG), we fitted separate linear mixed-effects models using
698 the lmer() function in the R package lme4 (version 1.1.33). The response variables in these
699 models were the frequencies of each *Ace* allele. For the malathion-treated cages, we modeled *Ace*
700 allele frequency changes over two distinct time periods: (1) from July 26, 2021, to September 21,
701 2021, when populations were evolving under malathion treatment, and (2) from September 21,
702 2021, to December 22, 2021, after malathion treatment had ceased. In contrast, for the
703 malathion-untreated cages, we assessed *Ace* allele frequency changes from the beginning of the
704 treatment to the end of the experiment, from July 26, 2021 to December 22, 2021.
705

706 **Model *Ace* allele frequency evolution**

707

708 We simulated the evolution of *Ace* allele frequencies and malathion resistance in our mesocosm

709 experiments using a viability selection model[52]. Additionally, based on the changes in *Ace* allele

710 frequencies in malathion-free environments across both sets of cages, we estimated the possible

711 ranges for the fitness costs of and dominance of malathion resistance.

712

713 <u>The impact of viability on *Ace* allele frequency dynamics and malathion resistance in the field</u>

714 <u>mesocosm experiment</u>

715 We investigated whether selection acting on viability recapitulates the allele frequency

716 and malathion resistance dynamics observed in the field. We focused on viability as it is a key

717 fitness-related trait in both malathion-rich and malathion-free environments. Furthermore, we

718 had laboratory measurements of viabilities for *Ace* genotypes across ranges of malathion

719 concentrations, allowing us to parametrize our model and test its predictions.

720 Within our model, the population frequencies of the *Ace* alleles change only due to selection that

721 acts on viability. We assumed that the effects of other forces (mutation, recombination, and

722 genetic drift) were negligible in comparison over the timescales that we considered (~10

723 generations). Under these assumptions, the frequency dynamics of the sensitive (f_0) and resistant

724 (f_1, f_2, f_3) *Ace* alleles follow from

725 $$f_i(t+1) = \frac{f_i(t)\sum_j w_{ij} f_j(t)}{\overline{w}(t)},$$

726 where t is time measured in generations, w_{ij} is viability of individuals carrying both i and j

727 alleles, and $\underline{w}$ is the mean population viability defined as

728 $$\overline{w}(t) = \sum_{i,j} f_i(t) f_j(t) w_{ij}.$$

729 We used laboratory measurements to determine individual viabilities w_{ij} in the absence
730 and presence of malathion (at 2.5 and 7.5 ppm). We used the marginal mean values from the
731 linear model for viability for each genotype and the predicted viability values from the dose-
732 response analysis (see previous section on 'Statistical analysis of fitness-associated phenotypes').
733 Due to the lack of measurements for heterozygous resistant genotypes, we assumed that
734 combinations of resistant alleles are codominant, i.e. that $w_{12} = 0.5 \cdot w_{11} + 0.5 \cdot w_{22}$; $w_{13} = 0.5 \cdot$
735 $w_{11} + 0.5 \cdot w_{33}$; $w_{23} = 0.5 \cdot w_{22} + 0.5 \cdot w_{33}$. The initial *Ace* allele frequencies, $f_i(0)$, were
736 estimated as the median values from the first sampling time point (July 13, 2021) for each
737 treatment group.

738 To estimate *D. melanogaster* generation times at our eight sampling time points, we used
739 a degree-day model based on Behrman and Schmidt[53]. This model assumes *D. melanogaster*
740 requires 112 degree-days to complete one generation, with development occurring between 12°C
741 and 29°C. We calculated daily degree-days as [(daily max. temp. + daily min. temp.) / 2] - 12°C,
742 adjusting temperatures outside the 12-29°C range to these limits. Cumulative degree-days were
743 tracked, with each 112 degree-day accumulation marking a new generation. This allowed us to
744 estimate generations at each sampling time point throughout the experiment.

745 We then calculated the population resistance R as a weighted sum,

746 $$R(t) = \sum_{i,j} g_{ij}(t) w_{ij},$$

747 where $g_{ij}(t)$ are genotype frequencies and w_{ij} are the corresponding viabilities. The initial
748 genotype frequencies were estimated from the initial allele frequencies, assuming Hardy-
749 Weinberg equilibrium:

750 $$g_{ij}(0) = f_i(0) f_j(0).$$

751 The consequent genotype frequencies followed from the viability selection model,

$$g_{ij}(t) = \begin{cases} \frac{2f_i(t)f_j(t)w_{ij}}{\overline{w}}, i \neq j, \\ \frac{f_i(t)f_j(t)w_{ij}}{\overline{w}}, i = j. \end{cases}$$

Inferring the ranges of possible fitness costs and dominance coefficients from empirical allele frequency trajectories

To estimate the fitness cost and dominance of malathion resistance in the malathion-free environment, we analyzed the empirical frequency trajectories of these alleles in both the untreated and treated populations after the removal of malathion. This approach allowed us to constrain the range of possible parameters that could explain the observed frequencies of the resistant alleles in both the treated and untreated populations. Assuming the resistant alleles share the same selection (s) and dominance (h) coefficients, and further that the cost of resistance is small (s<<1), the frequency dynamics follow

$$\partial_t f = s(f \cdot (1-f) \cdot (f + h(1-2f))),$$

allowing us to find s that would be consistent with the observed slope $\partial_t f$ of the frequency trajectory for a given h[54].

To do that, we first bootstrapped the combined frequency trajectories of resistant alleles in individual cages within each treatment group 10,000 times. For each set of bootstrapped trajectories, we used linear regression (LinearRegression().fit function from the scikit-learn Python library[55] to infer their slope. For a range of $h \in [0,1]$, we then calculated the bounds on s by finding the values that correspond to the lower and upper bound of the 95% confidence interval of the bootstrap distribution. To further constrain the range of possible parameters, we similarly inferred the full distribution of s for each set of cages, and evaluated their overlap by computing the joint likelihood function,

774 $$\mathcal{L} = \prod p(s),$$

775 where $p(s)$ is the probability density corresponding to a fixed value of s. Larger values of L

776 therefore correspond to more likely combinations of h and s given the observed frequency

777 dynamics.

778

779 **Characterize extent of forward and reverse sweep caused by *Ace* resistant alleles**

780 To assess how fluctuating organophosphate selection on the R2 and R3 *Ace* resistant alleles

781 affected genome-wide frequency trajectories of linked SNPs during and post-malathion

782 treatment, we employed a two-step approach. First, we used quasibinomial logistic regression to

783 estimate allele frequency shifts for genome-wide SNPs during malathion treatment (July 26 to

784 September 21, 2022) and post-treatment (September 21 to December 22, 2021). Second, we

785 developed a linked SNP selection procedure using linkage information from the inbred lines to

786 identify SNPs linked (Ace-linked) and not linked (control) to the sweeping R2 and R3 *Ace*

787 alleles across the genome. We used these sets of SNPs to quantify the extent of both the forward

788 *Ace* sweep during malathion treatment and the reverse *Ace* sweep post-treatment.

789

790 <u>Quasi-binomial logistic regression to estimate allele frequency differences in malathion-treated</u>

791 <u>and untreated populations during and after the malathion treatment</u>

792 To quantify allele frequency changes during malathion treatment (July 26 to September

793 21, 2022) and post-treatment (September 21 to December 22, 2021) in both treated and untreated

794 populations, we used a quasibinomial logistic regression approach[14,56]. This method models the

795 number of reads mapped to the alternative allele 'α' (relative to the reference allele 'A') at each

796 biallelic SNP for each pooled sample. To account for both the expected accuracy of HAFs as

797 well as pseudo-replication due to a fixed number of individuals in each sample [57], we estimated

798 an effective read depth reads (at each biallelic SNP for each pooled sample per population using

799 $$n_{eff} = \frac{\left((2 \times N \times EC) - 1\right)}{2 \times N + EC}$$

800 where N is the number of individuals per sample (100) and EC is the expected effective read

801 coverage based on the accuracy of HAF-pipe.

802 We then used a logit link implemented in a quasi-binomial logistic regression to model the

803 counts of the alternative allele 'α' $(C_a = HAF * neff)$ and reference allele 'A' $(C_A = (1 -$

804 $HAF) * neff)$ as a function of time in the malathion-treated and -untreated populations

805 $$logit(p_a) = log\left(\frac{p_a}{1 - p_a}\right) = b_0 + b_1 \times time + e$$

806 where p_a is probability of observing the allele 'α', while the coefficients b_0 and b_1 correspond to

807 the intercept and the effect of time, respectively. We fitted the model using the glm() function in

808 R (version 4.2.2) with family = 'quasibinomial'. To compute the allele frequency change (effect

809 size) between two time points (x_1 and x_2), we calculated

810 $$\Delta p = p_2 - p_1 = \frac{e^{(b_0 + b_1 \times x_2)}}{1 + e^{(b_0 + b_1 \times x_2)}} - \frac{e^{(b_0 + b_1 \times x_1)}}{1 + e^{(b_0 + b_1 \times x_1)}}$$

811

812 <u>Analysis of allele frequency changes of Ace-linked SNPs</u>

813 To quantify the extent of the forward and reverse *Ace* sweeps, we identified SNPs linked

814 to the sweeping R2 and R3 *Ace* alleles (*Ace*-linked), as well as unlinked (control) SNPs, using

815 whole genome data from the 76 sequenced Pennsylvania inbred lines (LNPA). First, we labeled

816 R2 and R3 *Ace* alleles as "R" and the remaining alleles (R1 and S) as "S", creating a binary

817 "R"/"S" *Ace* locus across the inbred lines. Among the inbred lines, 54 were homozygous "S", 5

818 heterozygous "R/S", and 17 homozygous "R". To select linked SNPs, we used the inbred lines

819 data to compute r2 between the binary "R"/"S" *Ace* locus and every reported biallelic SNP in the

820 inbred LNPA lines as the squared correlation coefficient of allelic indicator variables[58]. We
821 initially retained SNPs with r2 > 0.03, a threshold frequency previously used to deem two loci
822 highly linked[15]. However, to avoid issues with low-frequency SNPs in finite populations, we
823 added an allele count condition. We selected SNPs with $r^2 > 0.03$ that also have an allele present
824 in ≥60% of "R/R" lines and in ≤40% of "S/S" and "S/R" lines. This ensures selection of high-
825 frequency, well-assorted SNPs between "R" and "S" lines, which are more informative for sweep
826 analysis. This approach yielded 5672 *Ace*-linked SNPs across chromosomes 2, 3, and X. The
827 60% threshold was chosen as the highest value providing enough *Ace*-linked SNPs to uniformly
828 cover the genome, with consistent results when varied. Additionally, for each *Ace*-linked SNP,
829 we selected an unlinked control SNP with $r^2 < 0.01$ with the binary "R"/"S" *Ace* locus. To ensure
830 comparable initial conditions, unlinked control SNPs were chosen within 500kb of their linked
831 counterpart and had an allele frequency within 0.05 of the *Ace*-linked SNP at the start of
832 malathion treatment in each cage. Finally, to ensure that we track the SNP alleles that are linked
833 specifically with the resistant lines, we transformed the alleles frequencies based on the sign of r
834 — the non-squared correlation coefficient of allelic indicator variables. If r between *Ace* and a
835 SNP is positive, then the alternative allele is assorted together with the resistant *Ace* alleles in the
836 inbred lines, if the sign of r is negative, then the reference allele is linked to resistant *Ace* alleles,
837 and in this case the alternative/reference labels were flipped, and the allele frequencies f_t were
838 transformed to 1-f_t. This process yielded 4793 matched unlinked control SNPs, fewer than the
839 linked SNPs due to the stringent matching criteria. To visualize the results, we aggregated SNPs
840 into 1Mb windows along the genome and used bootstrap resampling to compute median GLM-
841 estimated effect sizes and confidence intervals for *Ace*-linked and unlinked control SNPs
842 separately for both forward and reverse sweeps. We excluded the areas around the centromeres

843 and chromosome ends where less than 20 *Ace*-linked or control SNPs were observed. To
844 characterize the width of each sweep, we performed a two-sample Mann-Whitney U-test within
845 every 1Mb window across the chromosome and recorded the width of the contiguous range of
846 windows around *Ace* in which the median for *Ace*-linked SNPs is significantly greater than the
847 median for control SNPs at the 0.05 confidence level.

848 To quantify the reversal phenomenon during the *Ace* sweep post-malathion treatment, we
849 analyzed allele frequency changes for the same Ace-linked and unlinked control SNPs during the
850 post-treatment period (September 21 to December 22, 2021). We binned SNPs into
851 500Kb windows based on the genomic distance from the *Ace* locus on chromosome 3R and then
852 compared post-treatment to during-treatment frequency changes by plotting them against each
853 other within each bin. To quantify the reversal, we performed a joint linear regression for *Ace*-
854 linked and control SNPs and recorded which bins have shown a slope for *Ace*-linked SNPs
855 significantly more negative compared to control at the 0.05 confidence level.

856

857 **Data and Code availability**

858 The data and associated code for this study will become available after manuscript acceptance in
859 public repositories: Dryad (https://doi.org/10.5061/dryad.w0vt4b937) for the data and GitHub
860 (https://github.com/mkarageorgi/Beneficial_Dominance_Reversal) for the code. The sequences
861 of the LNPA inbred lines used to construct the baseline *D. melanogaster* population for the field
862 mesocosm experiment are available on NCBI under accession ID PRJNA722305. The raw
863 sequencing reads for pooled samples from the malathion-treated cages, collected during the field
864 mesocosm experiment, will be deposited in the SRA BioProject under accession number
865 PRJNA1031645. The raw sequencing reads for pooled samples from the untreated cages are
866 already available in the same SRA BioProject (PRJNA1031645).

Extended Data Figure 1

a

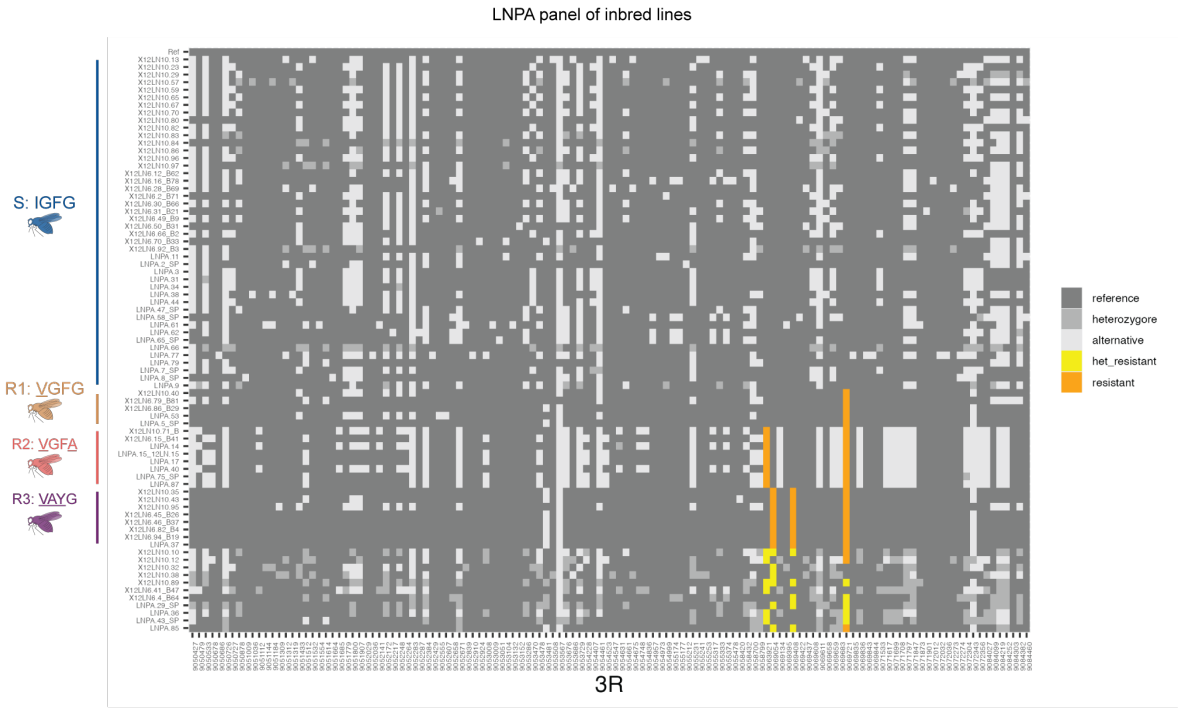

b

Ace haplotype	LNPA relative frequency (%)	DGRP relative frequency (%)
IGFG	63.16	54.15
VGFA	13.16	0.49
VAYG	12.50	30.73
VGFG	7.89	12.20
IGYG	1.32	0.98
IGFA	0.66	NA
VAFG	0.66	NA
VAYA	0.66	NA
IAFG	NA	1.46

Extended Data Figure 1. Sensitive and resistant *Ace* alleles in the panel of LNPA and DGRP inbred lines. a, Heatmap showing clustering of seventy-six *D. melanogaster* isogenic lines in the LNPA panel based on the sensitive or resistant *Ace* allele they carry (Ace-S: IGFG, Ace-R1: VGFG, Ace-R2: VGFA, Ace-R3: VAYG). The x-axis in the heatmap shows the genomic position on chromosome 3R around the *Ace* locus. Each row represents the *Ace* haplotype information of one isogenic line. Each column represents one biallelic exonic SNP at the *Ace* locus. Reference alleles are colored in dark grey, alternative alleles are colored in light grey, heterozygotes in medium grey. For the resistance mutations, alleles coding for the resistance mutations are colored in orange, alternative in grey, and heterozygotes in yellow. **b,** Table showing frequency of the sensitive and each of the resistant *Ace* alleles carrying different resistance haplotypes in the panels of LNPA and DGRP inbred lines.

Extended Data Figure 2

a

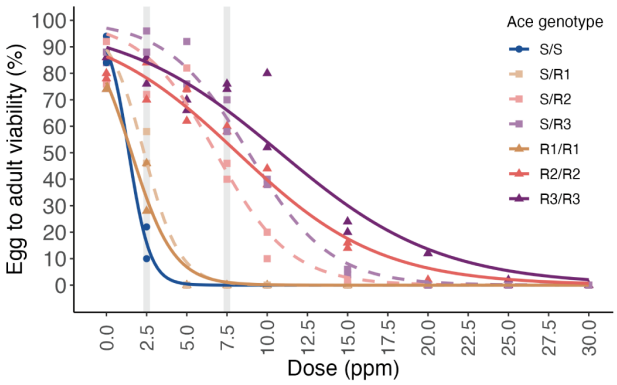

b

Dose response curve analysis for each Ace genotype

Genotype	LD50	std.error	statistic	p.value
SS	1.39	0.18	7.79	3.7768e-12
R1R1	1.56	0.20	7.68	6.3407e-12
R2R2	8.16	0.40	20.41	7.7563e-40
R3R3	10.81	0.45	23.96	3.3625e-46
SR1	2.34	0.19	12.49	3.0000e-23
SR2	6.80	0.26	25.89	2.1374e-49
SR3	8.84	0.30	29.95	1.3764e-55

Extended Data Figure 2. Comparison of malathion resistance among the *Ace* genotypes. a, Lab measurements of egg to adult viability in recombinant populations carrying different *Ace* genotypes on standard Drosophila media with a range of malathion concentrations (n= 2 technical replicates per genotype for each malathion doses, 50 eggs per replicate). Four-parameter logistic models fitted to data of each *Ace* genotype. The shaded areas highlight viability of each genotype at malathion doses (2.5ppm and 7.5 ppm) applied in the field mesocosm experiment. **b,** Table with estimated LD_{50} values for each *Ace* genotype from four-parameter logistic dose-response model (see also **Methods**).

Extended Data Figure 3

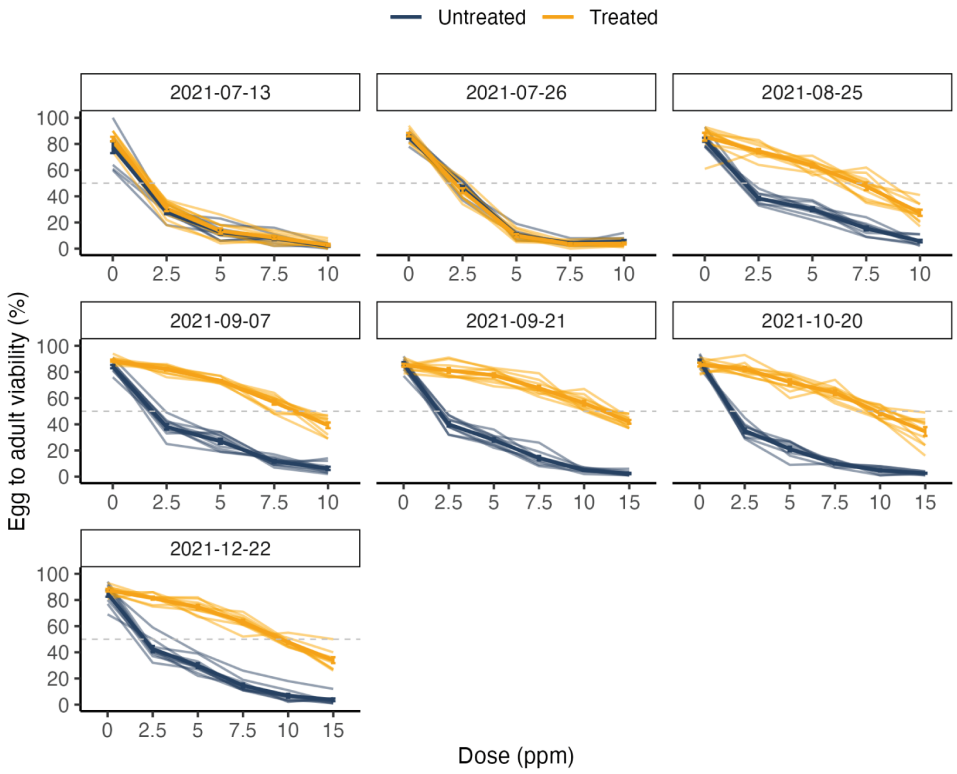

871

Extended Data Figure 3. Tracking evolution of malathion resistance in the field mesocosm experiment. Egg-adult survival on diets with a range of malathion concentrations as measured after two generations of common garden rearing throughout the field mesocosm experiment. Light lines and points show the mean egg-adult survival for individual malathion-treated (orange) and untreated (blue) populations (n = 2 technical replicates, 50 eggs per replicate). Dark lines and points represent the mean ± s.e.m. from all populations for each treatment group (n = 10 populations per treatment group). Further information on experimental design can be found in **Methods**.

872

Extended Data Figure 4

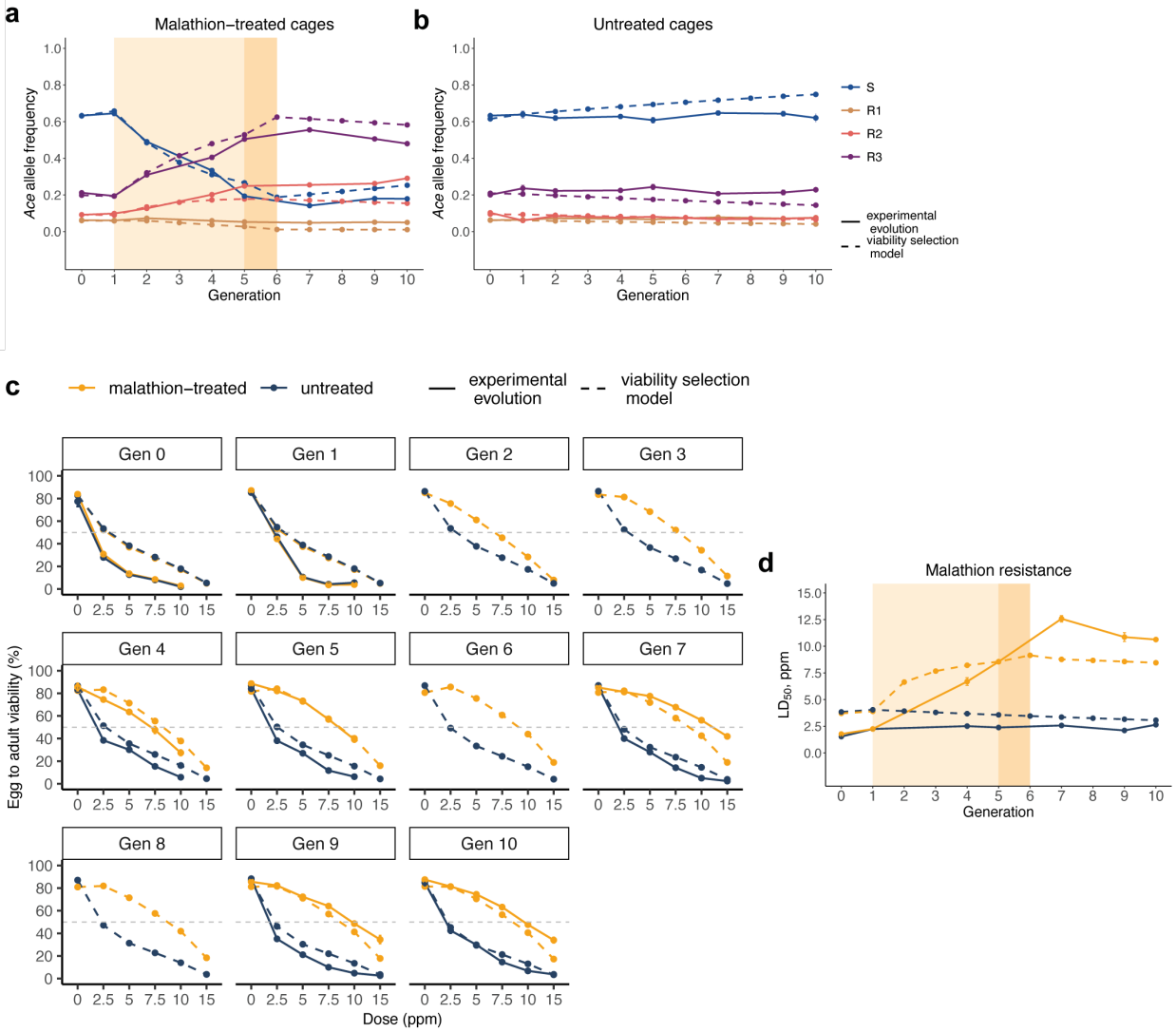

873

Extended Data Figure 4. Modeling the impact of viability selection on *Ace* allele frequency dynamics and malathion resistance in the field mesocosm experiment. **a-b,** Comparison between the observed *Ace* allele frequency trajectories over 10 generations in the malathion-treated (**a**) and untreated (**b**) populations from the field mesocosm experiment (mean ± s.e.m.) and the expected trajectories from simulations based on a viability selection model using laboratory-derived parameters. See **Methods** for details about the viability selection model. **c-d,** Comparison between the observed egg-to-adult survival across a range of malathion concentrations (**c**) and the evolution of malathion resistance (LD_{50}, ppm) (**d**) over 10 generations in the field mesocosm experiment (mean ± s.e.m.), and the expected results from the same model simulations. Dashed lines represent the expected values from the viability selection model, while solid lines represent the observed data from the field experiment. Generations were estimated based on a degree-day model starting from the first sampling point (July 13, 2021). In all plots, points correspond to each generation and estimated time point, and are connected by lines for visualization.

Extendend Data Table 1

Effect estimates from linear model analysis for LD50

Parameter	LD50	Std.Error	P.value
SS mean	1.39	0.19	-
SR1 mean	2.34	0.13	-
R1R1 mean	1.56	0.14	-
SS vs. SR1	-0.93	0.34	0.0063
SS vs. R1R1	-0.17	0.37	0.646
SR1 vs. R1R1	0.76	0.39	0.0516
SR1 - (SS + R1R1)/2 (additivity)	0.76	0.32	1e-16
(R1R1 - SS) / R1R1 (selection, s)	-0.25	0.29	0.751
(SR1 - SS) / (R1R1 - SS) (dominance, h)	-1.29	5.10	0.751
SR2 mean	6.80	0.24	-
R2R2 mean	8.16	0.36	-
SS vs. SR2	-5.38	0.36	0
SS vs. R2R2	-6.72	0.42	0
SR2 vs. R2R2	-1.34	0.45	0.003
SR2 - (SS + R2R2)/2 (additivity)	1.87	0.35	1e-16
(R2R2 - SS) / R2R2 (selection, s)	3.83	1.05	1e-16
(SR2 - SS) / (R2R2 - SS) (dominance, h)	0.78	0.06	1e-16
SR3 mean	8.84	0.32	-
R3R3 mean	10.81	0.49	-
SS vs. SR3	-7.41	0.36	0
SS vs. R3R3	-9.37	0.79	0
SR3 vs. R3R3	-1.96	0.80	0.0145
SR3 - (SS + R3R3)/2 (additivity)	2.59	0.48	1e-16
(R3R3 - SS) / R3R3 (selection, s)	5.64	1.45	1e-16
(SR3 - SS) / (R3R3 - SS) (dominance, h)	0.77	0.07	1e-16

874

Extendend Data Table 2

Effect estimates from logistic model analysis for viability

Parameter	Viability	Std.Error	Lower.CI	Upper.CI	P.value
SS mean	0.89	0.01	-	-	-
SR1 mean	0.86	0.02	-	-	-
R1R1 mean	0.76	0.02	-	-	-
SS vs. SR1	1.42	0.27	-	-	0.0702
SS vs. R1R1	2.61	0.47	-	-	<.0001
SR1 vs. R1R1	1.84	0.30	-	-	4e-04
SR1 - (SS + R1R1)/2 (additivity)	0.03	0.02	-0.02	0.07	0.214
(R1R1 - SS) / R1R1 (selection, s)	-0.15	0.03	-0.2	-0.09	0.001
(SR1 - SS) / (R1R1 - SS) (dominance, h)	0.29	0.20	-0.15	0.64	0.214
SR2 mean	0.87	0.02	-	-	-
R2R2 mean	0.74	0.02	-	-	-
SS vs. SR2	1.28	0.25	-	-	0.205
SS vs. R2R2	2.96	0.53	-	-	<.0001
SR2 vs. R2R2	2.31	0.39	-	-	<.0001
SR2 - (SS + R2R2)/2 (additivity)	0.05	0.02	0.01	0.1	0.027
(R2R2 - SS) / R2R2 (selection, s)	-0.17	0.05	-0.28	-0.09	0.001
(SR2 - SS) / (R2R2 - SS) (dominance, h)	0.17	0.15	-0.15	0.45	0.027
SR3 mean	0.86	0.02	-	-	-
R3R3 mean	0.78	0.02	-	-	-
SS vs. SR3	1.42	0.27	-	-	0.0702
SS vs. R3R3	2.43	0.44	-	-	<.0001
SR3 vs. R3R3	1.72	0.29	-	-	0.0018
SR3 - (SS + R3R3)/2 (additivity)	0.02	0.02	-0.02	0.06	0.286
(R3R3 - SS) / R3R3 (selection, s)	-0.13	0.02	-0.18	-0.08	0.001
(SR3 - SS) / (R3R3 - SS) (dominance, h)	0.32	0.19	-0.15	0.67	0.286

875

Extendend Data Table 3

Effect estimates from linear model analysis for fecundity

Parameter	Fecundity	Std.Error	Lower.CI	Upper.CI	P.value
SS mean	200.22	11.99	-	-	-
SR1 mean	165.33	14.01	-	-	-
R1R1 mean	136.50	14.86	-	-	-
SS vs. SR1	34.89	19.81	-	-	0.14
SS vs. R1R1	63.72	20.42	-	-	0.01
SR1 vs. R1R1	28.83	20.42	-	-	0.17
SR1 - (SS + R1R1)/2 (additivity)	-3.03	17.26	-36.62	31.59	0.879
(R1R1 - SS) / R1R1 (selection, s)	-0.32	0.09	-0.48	-0.12	0.003
(SR1 - SS) / (R1R1 - SS) (dominance, h)	0.55	0.40	-0.07	1.32	0.881
SR2 mean	187.60	13.64	-	-	-
R2R2 mean	167.78	14.37	-	-	-
SS vs. SR2	12.62	19.81	-	-	0.53
SS vs. R2R2	32.44	20.33	-	-	0.37
SR2 vs. R2R2	19.82	19.81	-	-	0.49
SR2 - (SS + R2R2)/2 (additivity)	3.60	18.42	-33.15	43.16	0.834
(R2R2 - SS) / R2R2 (selection, s)	-0.16	0.09	-0.33	0.03	0.093
(SR2 - SS) / (R2R2 - SS) (dominance, h)	0.39	4.09	-2.3	3.23	0.842
SR3 mean	202.00	12.71	-	-	-
R3R3 mean	106.44	11.99	-	-	-
SS vs. SR3	-1.78	17.47	-	-	0.92
SS vs. R3R3	93.78	16.95	-	-	<.0001
SR3 vs. R3R3	95.56	17.47	-	-	<.0001
SR3 - (SS + R3R3)/2 (additivity)	48.67	12.84	22.41	73.56	1e-16
(R3R3 - SS) / R3R3 (selection, s)	-0.47	0.07	-0.59	-0.31	0.001
(SR3 - SS) / (R3R3 - SS) (dominance, h)	-0.02	0.19	-0.48	0.29	0.001

876

Extendend Data Table 4

Extended Data Table 4.1 Effect of time on malathion resistance (LD50) in treated cages

	During treatment				*After treatment*			
Predictors	**Estimates**	**std. Error**	**Statistic**	**p**	**Estimates**	**std. Error**	**Statistic**	**p**
Intercept	-3.02 ***	0.46	-6.58	**<0.001**	15.56 ***	1.09	14.29	**<0.001**
Time	2.48 ***	0.10	24.26	**<0.001**	-0.57 ***	0.14	-3.96	**0.001**
Random Effects								
σ^2	0.91				0.98			
τ_{00}	$0.00_{Treatment_Cage}$				$0.24_{Treatment_Cage}$			
ICC					0.20			
N	$10_{Treatment_Cage}$				$10_{Treatment_Cage}$			
Observations	40				30			
Marginal R^2 / Conditional R^2	0.938 / NA				0.302 / 0.441			
AIC	122.513				101.066			

** p<0.05 ** p<0.01 *** p<0.001*

Extended Data Table 4.2 Effect of time on malathion resistance (LD50) in untreated cages

	Beginning of treatment to end of experiment			
Predictors	**Estimates**	**std. Error**	**Statistic**	**p**
Intercept	2.27 ***	0.15	14.91	**<0.001**
Time	0.03	0.02	1.07	0.288
Random Effects				
σ^2	0.16			
$\tau_{00\ Treatment_Cage}$	0.03			
ICC	0.15			
$N_{Treatment_Cage}$	10			
Observations	59			
Marginal R^2 / Conditional R^2	0.017 / 0.166			
AIC	83.651			

** p<0.05 ** p<0.01 *** p<0.001*

877

Extendend Data Table 5

Extended Data Table 5.1 Effect of time on S (IGFG) frequency in treated cages

	During treatment				*After treatment*			
Predictors	**Estimates**	**std. Error**	**Statistic**	**p**	**Estimates**	**std. Error**	**Statistic**	**p**
Intercept	0.88 ***	0.02	49.15	**<0.001**	0.04	0.05	0.74	0.468
Time	-0.13 ***	0.00	-30.81	**<0.001**	0.02 *	0.01	2.64	**0.014**
Random Effects								
σ^2	0.00				0.00			
τ_{00}	0.00_{cage}				0.00_{cage}			
N	10_{cage}				10_{cage}			
Observations	50				30			
Marginal R^2 / Conditional R^2	0.951 / NA				0.194 / NA			
AIC	-148.876				-97.774			

** p<0.05 ** p<0.01 *** p<0.001*

Extended Data Table 5.2 Effect of time on R1 (VGFG) frequency in treated cages

	During treatment				*After treatment*			
Predictors	**Estimates**	**std. Error**	**Statistic**	**p**	**Estimates**	**std. Error**	**Statistic**	**p**
Intercept	0.08 ***	0.00	16.13	**<0.001**	0.04 **	0.01	3.09	**0.005**
Time	-0.00 ***	0.00	-4.05	**<0.001**	0.00	0.00	0.46	0.651
Random Effects								
σ^2	0.00				0.00			
τ_{00}	0.00_{cage}				0.00_{cage}			
ICC					0.25			
N	10_{cage}				10_{cage}			
Observations	50				30			
Marginal R^2 / Conditional R^2	0.251 / NA				0.005 / 0.250			
AIC	-276.043				-162.492			

** p<0.05 ** p<0.01 *** p<0.001*

Extended Data Table 5.3 Effect of time on R2 (VGFA) frequency in treated cages

	During treatment				*After treatment*			
Predictors	**Estimates**	**std. Error**	**Statistic**	**p**	**Estimates**	**std. Error**	**Statistic**	**p**
Intercept	0.01	0.01	0.93	0.356	0.14 **	0.04	3.39	**0.002**
Time	0.04 ***	0.00	13.93	**<0.001**	0.02 **	0.01	3.03	**0.006**
Random Effects								
σ^2	0.00				0.00			
τ_{00}	0.00_{cage}				0.00_{cage}			
N	10_{cage}				10_{cage}			
Observations	50				30			
Marginal R^2 / Conditional R^2	0.798 / NA				0.240 / NA			
AIC	-178.169				-107.043			

** p<0.05 ** p<0.01 *** p<0.001*

Extended Data Table 5.4 Effect of time on R3 (VAYG) frequency in treated cages

	During treatment				*After treatment*			
Predictors	**Estimates**	**std. Error**	**Statistic**	**p**	**Estimates**	**std. Error**	**Statistic**	**p**
Intercept	0.03	0.01	1.88	0.067	0.78 ***	0.05	15.18	**<0.001**
Time	0.09 ***	0.00	27.59	**<0.001**	-0.04 ***	0.01	-5.18	**<0.001**
Random Effects								
σ^2	0.00				0.00			
τ_{00}	0.00_{cage}				0.00_{cage}			
ICC	0.04							
N	10_{cage}				10_{cage}			
Observations	50				30			
Marginal R^2 / Conditional R^2	0.937 / 0.940				0.481 / NA			
AIC	-170.172				-96.128			

** p<0.05 ** p<0.01 *** p<0.001*

878

Extendend Data Table 6

Extended Data Table 6.1 Effect of time on S (IGFG) haplotype frequency in untreated cages

	Beginning of treatment to end of experiment			
Predictors	**Estimates**	**std. Error**	**Statistic**	**p**
Intercept	0.63 ***	0.02	39.49	**<0.001**
Time	0.00	0.00	0.21	0.838
Random Effects				
σ^2		0.00		
$\tau_{00\ cage}$		0.00		
ICC		0.03		
N_{cage}		10		
Observations		69		
Marginal R^2 / Conditional R^2		0.001 / 0.032		
AIC		-196.762		

** p<0.05 ** p<0.01 *** p<0.001*

Extended Data Table 6.2 Effect of time on R1 (VGFG) haplotype frequency in untreated cages

	Beginning of treatment to end of experiment			
Predictors	**Estimates**	**std. Error**	**Statistic**	**p**
Intercept	0.06 ***	0.00	14.68	**<0.001**
Time	0.00	0.00	1.91	0.061
Random Effects				
σ^2		0.00		
$\tau_{00\ cage}$		0.00		
N_{cage}		10		
Observations		69		
Marginal R^2 / Conditional R^2		0.051 / NA		
AIC		-370.061		

** p<0.05 ** p<0.01 *** p<0.001*

Extended Data Table 6.3 Effect of time on R2 (VGFA) haplotype frequency in untreated cages

	Beginning of treatment to end of experiment			
Predictors	**Estimates**	**std. Error**	**Statistic**	**p**
Intercept	0.07 ***	0.01	9.08	**<0.001**
Time	-0.00	0.00	-0.02	0.985
Random Effects				
σ^2		0.00		
$\tau_{00\ cage}$		0.00		
ICC		0.02		
N_{cage}		10		
Observations		69		
Marginal R^2 / Conditional R^2		0.000 / 0.024		
AIC		-285.686		

** p<0.05 ** p<0.01 *** p<0.001*

Extended Data Table 6.4 Effect of time on R3 (VAYG) haplotype frequency in untreated cages

	Beginning of treatment to end of experiment			
Predictors	**Estimates**	**std. Error**	**Statistic**	**p**
Intercept	0.24 ***	0.01	17.99	**<0.001**
Time	-0.00	0.00	-0.86	0.392
Random Effects				
σ^2		0.00		
$\tau_{00\ cage}$		0.00		
ICC		0.05		
N_{cage}		10		
Observations		69		
Marginal R^2 / Conditional R^2		0.010 / 0.064		
AIC		-222.940		

** p<0.05 ** p<0.01 *** p<0.001*

879

880 **References**

881 1. Dobzhansky, T. A review of some fundamental concepts and problems of population
882 genetics. *Cold Spring Harb. Symp. Quant. Biol.* **20**, 1–15 (1955).
883 2. Hedrick, P. W. Genetic variation in a heterogeneous environment. II. Temporal
884 heterogeneity and directional selection. *Genetics* **84**, 145–157 (1976).
885 3. Wittmann, M. J., Bergland, A. O., Feldman, M. W., Schmidt, P. S. & Petrov, D. A.
886 Seasonally fluctuating selection can maintain polymorphism at many loci via segregation
887 lift. *Proc. Natl. Acad. Sci. U. S. A.* **114**, E9932–E9941 (2017).
888 4. Di, C. & Lohmueller, K. E. Revisiting dominance in population genetics. *Genome Biol.*
889 *Evol.* **16**, 1–17 (2024).
890 5. Menozzi, P., Shi, M. A., Lougarre, A., Tang, Z. H. & Fournier, D. Mutations of
891 acetylcholinesterase which confer insecticide resistance in Drosophila melanogaster
892 populations. *BMC Evol. Biol.* **4**, 4 (2004).
893 6. Karasov, T., Messer, P. W. & Petrov, D. A. Evidence that adaptation in Drosophila is not
894 limited by mutation at single sites. *PLoS Genet.* **6**, e1000924 (2010).
895 7. Wright, S. Physiological and evolutionary theories of dominance. *Am. Nat.* **68**, 24–53
896 (1934).
897 8. Brian, C. & Hugues, K. A. The maintenance of genetic variation in life-history traits. in
898 *Evolutionary genetics* (eds. Singh, R. S. & Krimbas, C. B.) 369–392 (Cambridge University
899 Press, Cambridge, England, 2000).
900 9. Charlesworth, B. Causes of natural variation in fitness: evidence from studies of Drosophila
901 populations. *Proc. Natl. Acad. Sci. U. S. A.* **112**, 1662–1669 (2015).
902 10. Hedrick, P. W. Balancing selection. *Curr. Biol.* **17**, R230–1 (2007).

903 11. Hedrick, P. W. Genetic polymorphism in heterogeneous environments: The age of
904 genomics. *Annu. Rev. Ecol. Evol. Syst.* **37**, 67–93 (2006).
905 12. Bergland, A. O., Behrman, E. L., O'Brien, K. R., Schmidt, P. S. & Petrov, D. A. Genomic
906 evidence of rapid and stable adaptive oscillations over seasonal time scales in Drosophila.
907 *PLoS Genet.* **10**, e1004775 (2014).
908 13. Machado, H. E. *et al.* Broad geographic sampling reveals the shared basis and
909 environmental correlates of seasonal adaptation in Drosophila. *Elife* **10**, (2021).
910 14. Rudman, S. M. *et al.* Direct observation of adaptive tracking on ecological time scales in
911 Drosophila. *Science* **375**, eabj7484 (2022).
912 15. Bitter, M. C. *et al.* Continuously fluctuating selection reveals fine granularity of adaptation.
913 *Nature* **634**, 389–396 (2024).
914 16. Grant, B. S., Owen, D. F. & Clarke, C. A. Parallel rise and fall of melanic peppered moths
915 in America and Britain. *J. Hered.* **87**, 351–357 (1996).
916 17. Van't Hof, A. E. *et al.* The industrial melanism mutation in British peppered moths is a
917 transposable element. *Nature* **534**, 102–105 (2016).
918 18. Pfenninger, M., Foucault, Q., Waldvogel, A.-M. & Feldmeyer, B. Selective effects of a
919 short transient environmental fluctuation on a natural population. *Mol. Ecol.* **32**, 335–349
920 (2023).
921 19. Pfenninger, M. & Foucault, Q. Population genomic time series data of a natural population
922 suggests adaptive tracking of fluctuating environmental changes. *Integr. Comp. Biol.* **62**,
923 1812–1826 (2022).
924 20. Barrett, R., Rogers, S. M. & Schluter, D. Natural selection on a major armor gene in
925 threespine stickleback. *Science* **322**, 255–257 (2008).

21. Schluter, D. *et al.* Fitness maps to a large-effect locus in introduced stickleback populations. *Proc. Natl. Acad. Sci. U. S. A.* **118**, e1914889118 (2021).

22. Barrett, R. D. H. *et al.* Linking a mutation to survival in wild mice. *Science* **363**, 499–504 (2019).

23. Ludwig, A. *et al.* Twenty-five thousand years of fluctuating selection on leopard complex spotting and congenital night blindness in horses. *Philosophical Transactions of the Royal Society B: Biological Sciences* (2015) doi:10.1098/rstb.2013.0386.

24. Busoms, S. *et al.* Fluctuating selection on migrant adaptive sodium transporter alleles in coastal. *Proc Natl Acad Sci U S A* **115**, E12443–E12452 (2018).

25. Curtsinger, J. W., Philip M. Service & Prout, T. Antagonistic pleiotropy, reversal of dominance, and genetic polymorphism. *Am. Nat.* **144**, 210–228 (1994).

26. Grieshop, K., Ho, E. K. H. & Kasimatis, K. R. Dominance reversals: The resolution of genetic conflict and maintenance of genetic variation. *arXiv [q-bio.PE]* (2021).

27. Connallon, T. & Chenoweth, S. F. Dominance reversals and the maintenance of genetic variation for fitness. *PLoS Biol.* **17**, e3000118 (2019).

28. Wittmann, M. J., Mousset, S. & Hermisson, J. Modeling the genetic footprint of fluctuating balancing selection: from the local to the genomic scale. *Genetics* **223**, iyad022 (2023).

29. Johnson, O. L., Tobler, R., Schmidt, J. M. & Huber, C. D. Fluctuating selection and the determinants of genetic variation. *Trends Genet.* **39**, 491–504 (2023).

30. Kaplan, N. L., Hudson, R. R. & Langley, C. H. The 'hitchhiking effect' revisited. *Genetics* **123**, 887–899 (1989).

31. Hall, J. C. & Kankel, D. R. Genetics of acetylcholinesterase in Drosophila melanogaster. *Genetics* **83**, 517–535 (1976).

949 32. Aldridge, W. N. Some properties of specific cholinesterase with particular reference to the
950 mechanism of inhibition by diethyl p-nitrophenyl thiophosphate (E 605) and analogues.
951 *Biochem. J.* **46**, 451–460 (1950).
952 33. Miyo, T., Akai, S. & Oguma, Y. Seasonal fluctuation in susceptibility to insecticides within
953 natural populations of Drosophila melanogaster: empirical observations of fitness costs of
954 insecticide resistance. *Genes Genet. Syst.* **75**, 97–104 (2000).
955 34. Miyo, T., Oguma, Y. & Charlesworth, B. Seasonal fluctuation in susceptibility to
956 insecticides within natural populations of Drosophila melanogaster. II. Features of genetic
957 variation in susceptibility to organophosphate insecticides within natural populations of D.
958 melanogaster. *Genes Genet. Syst.* **81**, 273–285 (2006).
959 35. Kapun, M. *et al.* Drosophila Evolution over Space and Time (DEST): A new population
960 genomics resource. *Mol. Biol. Evol.* **38**, 5782–5805 (2021).
961 36. FAO. Pesticides use and trade, 1990–2022. (2024).
962 37. Mackay, T. F. C. *et al.* The Drosophila melanogaster Genetic Reference Panel. *Nature* **482**,
963 173–178 (2012).
964 38. Paaby, A. B., Bergland, A. O., Behrman, E. L. & Schmidt, P. S. A highly pleiotropic amino
965 acid polymorphism in the Drosophila insulin receptor contributes to life-history adaptation.
966 *Evolution* **68**, 3395–3409 (2014).
967 39. Shi, M. A. *et al.* Acetylcholinesterase alterations reveal the fitness cost of mutations
968 conferring insecticide resistance. *BMC Evol. Biol.* **4**, 5 (2004).
969 40. Langmüller, A. M. *et al.* Fitness effects for Ace insecticide resistance mutations are
970 determined by ambient temperature. *BMC Biol.* **18**, 157 (2020).
971 41. Tilk, S. *et al.* Accurate Allele Frequencies from Ultra-low Coverage Pool-Seq Samples in

972 Evolve-and-Resequence Experiments. *G3* **9**, 4159–4168 (2019).
973 42. Gillespie, J. H. A general model to account for enzyme variation in natural populations. V.
974 The SAS--CFF model. *Theor. Popul. Biol.* **14**, 1–45 (1978).
975 43. Taverner, A. M. *et al.* Adaptive substitutions underlying cardiac glycoside insensitivity in
976 insects exhibit epistasis in vivo. *Elife* **8**, (2019).
977 44. Guo, L. *et al.* Convergent resistance to GABA receptor neurotoxins through plant-insect
978 coevolution. *Nat. Ecol. Evol.* **7**, 1444–1456 (2023).
979 45. Mutero, A., Pralavorio, M., Bride, J. M. & Fournier, D. Resistance-associated point
980 mutations in insecticide-insensitive acetylcholinesterase. *Proc. Natl. Acad. Sci. U. S. A.* **91**,
981 5922–5926 (1994).
982 46. Harel, M. *et al.* Three-dimensional structures of Drosophila melanogaster
983 acetylcholinesterase and of its complexes with two potent inhibitors. *Protein Sci.* **9**, 1063–
984 1072 (2000).
985 47. Ritz, C., Baty, F., Streibig, J. C. & Gerhard, D. Dose-Response Analysis Using R. *PLoS*
986 *One* **10**, e0146021 (2015).
987 48. Miyo, T. & Oguma, Y. Negative correlations between resistance to three organophosphate
988 insecticides and productivity within a natural population of Drosophila melanogaster
989 (Diptera: Drosophilidae). *J. Econ. Entomol.* **95**, 1229–1238 (2002).
990 49. Singh, R. S. & Morton, R. A. Selection for malathion-resistance in Drosophila
991 melanogaster. *Can. J. Genet. Cytol.* **23**, 355–369 (1981).
992 50. Li, H. & Durbin, R. Fast and accurate short read alignment with Burrows-Wheeler
993 transform. *Bioinformatics* **25**, 1754–1760 (2009).
994 51. Kessner, D., Turner, T. L. & Novembre, J. Maximum likelihood estimation of frequencies

995 of known haplotypes from pooled sequence data. *Mol. Biol. Evol.* **30**, 1145–1158 (2013).
996 52. Gillespie, J. H. *Population Genetics*. (Johns Hopkins University Press, Baltimore, MD,
997 2004).
998 53. Behrman, E. L. & Schmidt, P. How predictable is rapid evolution? (2022)
999 doi:10.1101/2022.10.27.514123.
1000 54. Ewens, W. J. *Mathematical Population Genetics 1: Theoretical Introduction*. (Springer,
1001 New York, NY, 2010).
1002 55. Pedregosa, F. *et al.* Scikit-learn: Machine Learning in Python. *arXiv [cs.LG]* (2012).
1003 56. Wiberg, R. A. W., Gaggiotti, O. E., Morrissey, M. B. & Ritchie, M. G. Identifying
1004 consistent allele frequency differences in studies of stratified populations. *Methods Ecol.*
1005 *Evol.* **8**, 1899–1909 (2017).
1006 57. Feder, A. F., Petrov, D. A. & Bergland, A. O. LDx: estimation of linkage disequilibrium
1007 from high-throughput pooled resequencing data. *PLoS One* **7**, e48588 (2012).
1008 58. VanLiere, J. M. & Rosenberg, N. A. Mathematical properties of the r2 measure of linkage
1009 disequilibrium. *Theor. Popul. Biol.* **74**, 130–137 (2008).